LASER TRANSMISSION THROUGH SIMULATED CIRRUS CLOUDS

by Ila L. Kolb

William R. Cotton, P.I.

Colorado State University

DEPARTMENT OF ATMOSPHERIC SCIENCE

PAPER NO. 704

LASER TRANSMISSION THROUGH SIMULATED CIRRUS CLOUDS

by

Ila L. Kolb

Department of Atmospheric Science

Colorado State University

Fort Collins, CO 80523
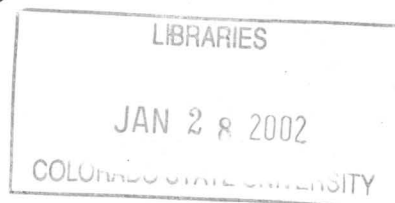
Summer 2001

Atmospheric Science Paper No. 704

ABSTRACT

Since approximately 20% of the globe is covered with cirrus clouds at any given time, it is clear that any airborne or spaceborne system using a laser will intercept cirrus clouds at some point. Cirrus clouds contain a very complex microphysical structure that will affect laser power by scattering and reflecting it away from the intended target, thus reducing efficiency and possibly even making it ineffective.

Using two thin cirrus laser transmission models, a single homogeneous cloud layer model and a multiple cloud layer model, laser transmission profiles are generated from a simulated cirrus cloud case created by the RAMS model.

Sensitivity studies are performed on the laser transmission model to examine the effects of aerosols and water vapor, ice crystal orientation, multiple scattering contributions, and the differences between the single and multiple layer models. Different parts of the RAMS simulated cloud are examined as well as the development of a particular cloud feature. The two different laser transmission models are compared against each other for a variety of different cirrus cloud conditions within the simulated case.

Optical depth is a cloud variable that is fairly well measured using remote sensing techniques and airborne lidar. Average optical depth is examined as a viable parameter to indicate the likely transmission through a cloud.

This case study offers a basis for an atmospheric decision aid for airborne and spaceborne laser systems of when to attempt to penetrate cirrus clouds.

Ila L. Kolb
Department of Atmospheric Science
Colorado State University
Fort Collins, Colorado 80523
Summer 2001

ACKNOWLEDGEMENTS

CONTENTS

Chapter 1

INTRODUCTION

1.1 Motivation

A laser beam propagating through the atmosphere can be attenuated, broadened, defocused, and possibly even deflected from its original direction. These atmospheric effects are caused by a variety of constituents found in the atmosphere including molecules, aerosols, water vapor, cloud droplets, ice crystals, and precipitation drops. Optical turbulence and gases are other cause of attenuation of a laser beam in the atmosphere that is not related to particles. All of these effects have a great impact on the use of lasers for a variety of applications including optical communication, weaponry, target designation, ranging, remote sensing, and other applications that require the transmission of lasers through the atmosphere (Weichel 1989). Clearly these affects need to be understood.

There has been a great deal of work done on understanding how molecules, aerosols, water vapor, cloud droplets, precipitation drops (Weichel 1989, Liou 1992, and Stephens 1994) and optical turbulence (Masson et al. 1996, Eaton et al. 1998, and Hahn et al. 1999) interact with a laser beam. Optical turbulence is a difficulty to overcome but is still being researched. The aerosols and other particles have fairly constant radiative properties depending on their concentration and size distributions and are fairly well understood. Ice crystals have also been well studied but they have often been simplified to ice spheres (Takano and Liou 1989a). Due to the wide range of shapes of ice crystals and aggregates, laser beam transmission through clouds containing ice crystals, such as cirrus clouds, has not been modeled well.

1.2 Cirrus Clouds

Cirrus clouds pose a very complex problem for airborne, spaceborne, and even ground-based laser systems due to their location at high altitudes, thin nature, and non-blackness. They are also global in nature, being present at all latitudes regardless of land or sea surface or season of the year (Liou 1986). Cirrus clouds frequently occur in thin sheets of great horizontal dimensions, hundreds or even thousand of kilometers, are relatively stable, and can persist for very long time periods. They are often associated with large scale disturbances such as the cirrus anvils related to cumulus convection encountering a stable layer (the tropopause), or the cirrus clouds that form in the area of a jet stream which are associated with small-scale vertical circulations around the jet (Cotton and Anthes 1989).

Cirrus clouds also have complex microphysics and a variety of ice habits. The composition of cirrus clouds was first sampled by Weickmann (1945) and was determined to predominantly contain columnar crystals. Later studies (Heymsfield and Knollenburg 1972, Hobbs et al 1975, Varley et al. 1980) showed that different types of cirrus clouds (cirrostatus, cirrocumulus, and cirrus uncinus) had a variety of ice habits of different proportion. The ice habits found in cirrus include columns, column bundles, bullet rosettes, bullets, plates, and thick plates (Liou 1992).

In the past, radiative transfer calculations for ice crystals have assumed spherical particles for non-spherical particles. Liou (1972) made the first attempt to model the single scattering properties of long circular cylinders. This worked better than spherical particles in modeling radiative properties but the hexagonal structure of ice crystals was still missing. Takano and Liou (1989a) used a ray-tracing technique to develop a light scattering and absorption program for hexagonal columns and plates accounting for different ice crystal size distribution and orientation. This work continued (Takano and Liou 1995) to include hollow columns, bullet rosettes, dendrites, and capped columns. The culmination of this work is a thin cirrus laser transmission model that takes into account

different size and shape distributions as well as aerosols, water vapor, and air molecules (Liou et al. 2000).

Simulations have been run with this model for standard values of different types of cirrus clouds (Liou et al. 2000), such as cirrus uncinus, cirrostratus, cold cirrus, and contrails. A realistic case of an actual observed cloud or a realistic simulated case has not yet been examined with this model.

1.3 RAMS Cirrus Simulations

The RAMS (Regional Atmospheric Modeling System; Pielke et al. 1992) model offers detailed microphysical information on clouds of many types. Different cirrus cloud simulations have been run using the RAMS model, some hypothetical and some based on actual clouds from different field campaigns (Benedetti and Stephens 2001, Cheng et al. 2001, Clark et al. 1999). These simulations run with the Harrington et al. (1999) two-stream radiation and two-moment microphysics scheme (Harrington et al. 1995) offer very detailed optical property information. Optical properties such as single scatter albedo, extinction, and optical depth are given for every grid point within the cloud domain. Using this information, it is possible to average the values to create a 1-D homogeneous layer or a series of homogeneous layers of cloud and input it into the laser transmission model developed by Liou et al. (2000). This will result in a series of laser transmission profiles for different types and conditions of cirrus clouds.

A RAMS simulation for thin cirrus was generated for a cloud observed in the FIRE (First ISCCP (International Satellite Cloud Climatology Project) Regional Experiment II field campaign during November of 1991. This simulation compared reasonably well with the observations from the experiment (Wu et al. 1999) and can therefore be used as a realistic case. Though the microphysics and ice habits were not simulated exactly, the RAMS simulated cloud structure provides useful data for simulating laser transmission through a time and space-varying cloud field.

The RAMS simulation is averaged using a weighted-averaging scheme to transform the simulated cloud information into something that the thin cirrus transmission code can

use. Boxes of constant size are used to average the cloud to choose features of interest. Vertical profiles of temperature, pressure, relative humidity, and mixing ratio from RAMS are utilized in the transmission code to make the case more realistic. Layer averages of single scatter albedo, extinction and transmission are given as input for the optical cloud properties to the laser transmission code.

1.4 Objectives

The aim of this work is to examine a realistic case of laser transmission through simulated cirrus clouds. This is accomplished by looking at transmission through different parts of a RAMS-generated cirrus cloud and looking at a specific feature as it develops. The importance of resolving vertical structure in the laser transmission model is also examined by comparing two laser transmission models, single layer and multiple layer models, with differing vertical resolution. A plot of all the transmission data for both single layer and multiple layer transmission models is then compared to the average optical depth to see if there is any strong correlation.

In chapter two, information on RAMS and the cirrus case used for this work are provided, while in chapter three the laser transmission models are described.

In chapter four, the results from sensitivity studies of the laser transmission models offers justification for the way the the laser model was set up for the transmission runs. Chapter five examines the results from the two laser transmission models and the use of a 1-D homogeneous cloud layer model is compared to the vertical structure of a multi-layer model.

Summary and conclusions as well as suggestions for future research are included in chapter six.

Chapter 2

THE RAMS CASE

2.1 Introduction to RAMS

The thin cirrus simulation used in this work was generated by RAMS version 3b with interactive nested grids. A general description of the RAMS model can be found in Pielke et al. (1992). A two-moment microphysical parameterization scheme described by Meyers (1997) is used to predict the mixing ratios and number concentrations of pristine ice crystals, snow, and aggregates. By coupling the two-moment cloud microphysics to the two-stream radiation model (Harrington et al. 1999), the ice habit of the ice particles in the radiative transfer equations can be accounted for. The addition of these schemes allows for the calculation of optical properties such as optical depth, single scatter albedo, and extinction for the mesoscale simulation of the 26 November 1991 cirrus event.

2.2 Model Set Up

The RAMS atmospheric variables were initialized with a combination of MAPS (Mesoscale Analysis and Prediction System) analysis data, a product of NOAA (National Oceanic and Atmospheric Administration) Forecast Systems Laboratory, and National Weather Service rawinsonde data from 0000 UTC 26 November 1991. The mesoscale nested grid simulation was run with 4 grids with a plot of the first 3 grids shown in Figure 2.1; grid 2 was used for this work.

Table 2.1 shows the model set up and Table 2.2 shows the vertical levels used. A vertical spacing of 500 m is used near the model top and at the surface while a spacing of 200 m is used within the cloud layer.
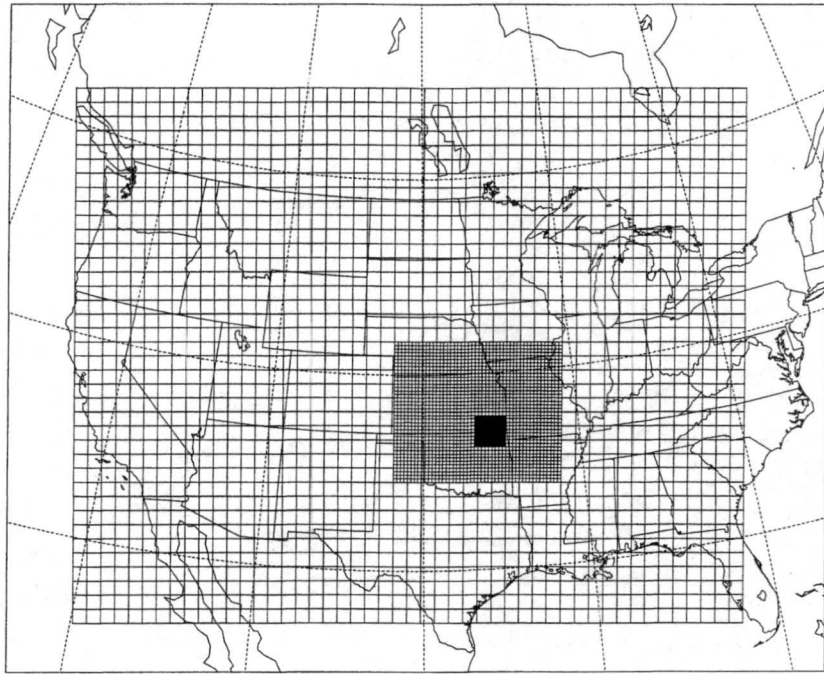
Figure 2.1: The mesoscale grid configuration for grids 1, 2, and 3.

The model is initialized with only one grid, grid 1 (the coarsest grid), and two-way interactive nesting is used for the other grids. Grid 2 is spawned 6 hours into the simulation, grid 3 is activated at 12 hours into the simulation, and grid 4 is spawned at 16 hours. The grids are set up to examine a weak cloud band associated with the leading portion of the observed cloud system.

2.2.1   26 November 1991 case

The case of interest occurred during the FIRE (First ISCCP (International Satellite Cloud Climatology Project) Regional Experiment) II field experiment during November of 1991. The thin cirrus event occurred on 26 November 1991 from 1600 UTC to 0000 UTC 27 November 1991 and is well documented by Mace et al. (1995). This experiment provided a variety of different observing systems to compare the simulation against and offered a great case to simulate. The synoptic situation on 26 November 1991 was characterized by a small amplitude upper-level trough-ridge system over North America, with northwesterly flow in the upper-levels ahead of the offshore ridge over the West Coast, and a broad diffluent trough in the central United States. The exit region of a strong upper-level

Table 2.1: Model set up for mesoscale grids. The vertical same for every grid.

	Case 1
number of grids	4
x grid points	50, 50, 47, 46
y grid points	40, 42, 47, 46
z grid points	65, 65, 65, 65
horizontal grid spacings (km)	80, 20, 4, 1
vertical grid spacings (m)	200 to 500

Table 2.2: Vertical levels used in the mesoscale simulation (in m).

0.0	300.0	600.0	900.0	1200.0	1500.0
1800.0	2100.0	2400.0	2700.0	3000.0	3300.0
3600.0	3900.0	4100.0	4300.0	4500.0	4700.0
4900.0	5100.0	5300.0	5500.0	5700.0	5900.0
6100.0	6300.0	6500.0	6700.0	6900.0	7100.0
7300.0	7500.0	7700.0	7900.0	8100.0	8300.0
8500.0	8700.0	8900.0	9100.0	9300.0	9500.0
9700.0	9900.0	10100.0	10300.0	10600.0	10900.0
11200.0	11500.0	11800.0	12200.0	12600.0	13000.0
13400.0	13800.0	14200.0	14600.0	15000.0	15500.0
16000.0	16500.0	17000.0	17500.0	18000.0	

northwesterly jet over the central United States contributed to the development of the cirrus cloud system examined in this work. A more detailed description of this particular event is found in Mace et al. (1995). Figure 2.2 shows GOES-7 infrared imagery of the cirrus band during the last few hours of the RAMS simulation.

Figure 2.3 shows the 500 hPa geopotential height at 24 hours (0000 UTC 27 November 1991) into the simulation from grid 1 as well as the 500 hPa geopotential height from the MAPS analysis. The model appeared to capture the large-scale trough-ridge pattern reasonably well with the the trough perhaps not being quite as deep as the observations. Figure 2.4 shows the simulated 7600 m (above sea-level) total ice concentration (pristine ice, snow, and aggregates), from grid 2 as well as modeled cloud optical depth from 18 hours into the simulation and observed optical depth derived from satellite observations from 1800 UTC 26 November 1991. It appears that the model reproduced cloud bands
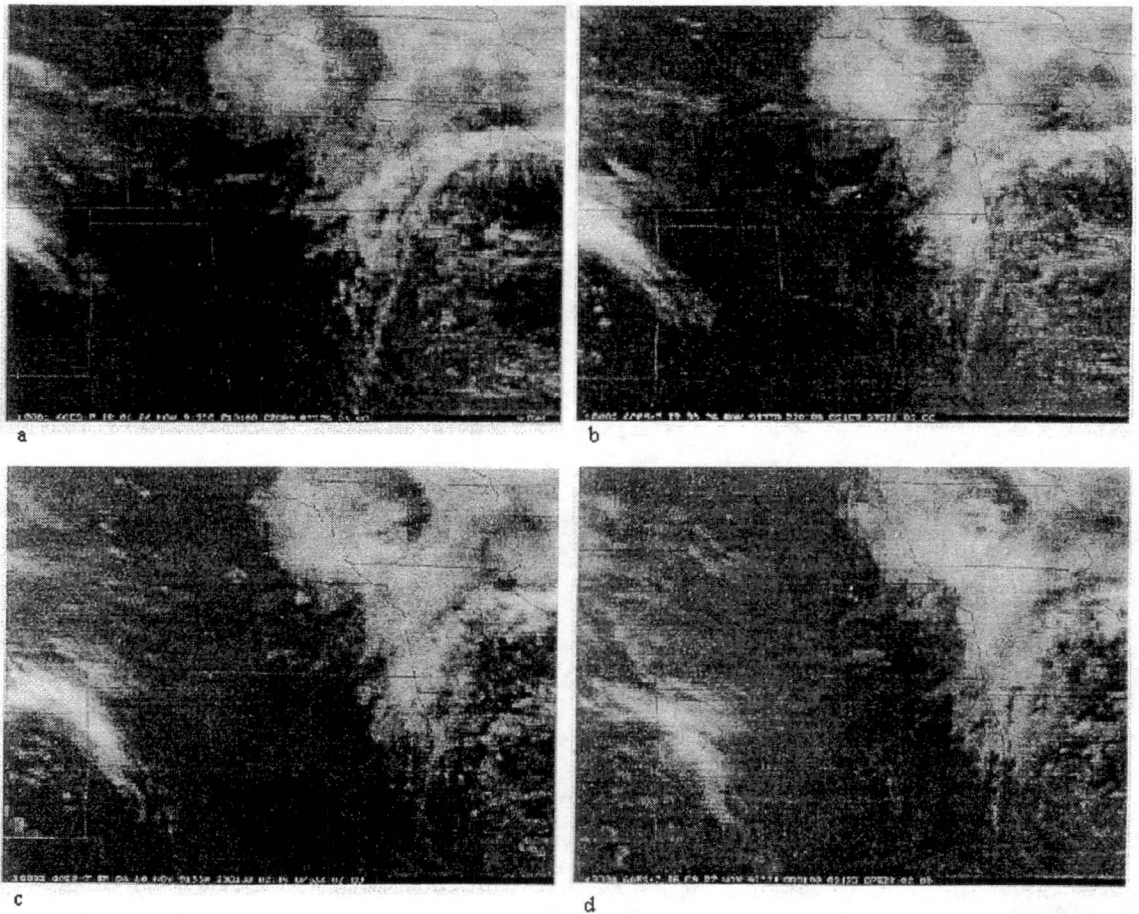
Figure 2.2: GOES-7 infrared imagery showing the progression of the 26 November 1991 cirrus event at (a) 2100 UTC 26 Nov 91; (b) 2200 UTC 26 Nov 91; (c) 2300 UTC 26 Nov 91; and (d) 0000 UTC 27 Nov 91.

that are consistent with the high cloud visible optical depth maxima derived from satellite data, from Mace et al. (1995). The simulated cirrus band, however, appears to be more to the northwest than the satellite-derived cirrus band. The model-derived cloud optical depth, from solar band 3: 0.245 - 0.7 μm, calculated from the two-stream radiation scheme appears to compare well with the results of Mace et al. (1995). According to Wu (1999) and Cheng et al. (2001), RAMS showed reasonable skill in simulating the 26 November 1991 cirrus event and the results can be used as a realistic thin cirrus case.
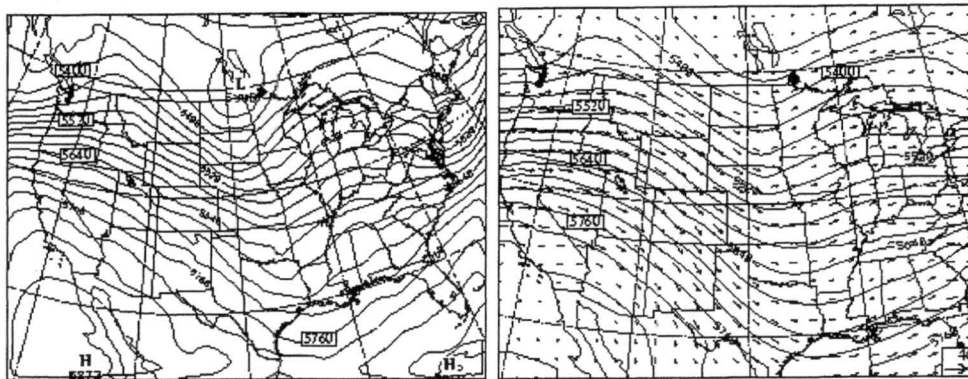
(a)   (b)

Figure 2.3: (a) 500 hPa geopotential height (at contour intervals of 30 m) from MAPS analysis at 0000 UTC 27 Nov 91 and (b) 24 hour predicted 500 hPa geopotential height (at contour intervals of 30 m) with 500 hPa wind vectors (m/s) from grid 1 of the mesoscale simulation at 24 hours into the simulation. Inset indicates the scale of the wind vectors.

2.3 Averaging Scheme

2.3.1 Method

To fit the RAMS optical variables: optical depth, single scatter albedo and extinction, and atmospheric variables: temperature, pressure, relative humidity, and mixing ratio, into the laser transmission model it is necessary to average the data to one-dimensional layers. It is important to know how this is done since variations in the averaging scheme can cause widely different results. The RAMS output was weight-averaged with the mass of the grid volume between two cloud defined levels within the cloud. For both the single and multiple layer models a series of 120 km by 120 km boxes were chosen in the horizontal to average within. Figure 2.5 shows a single time plot of optical depth with all of the averaging boxes plotted over it. As the cloud proceeds to the east, cloud fills the boxes to the right of the plot. This offers a large area of cloud to examine and offers a horizontal sweep distance that the laser model can look through. These boxes were chosen to have cases of cloud only and cloud with clear air. Boxes that have mostly clear air with little cloud have the possibility of errors in the optical properties. Such boxes should be treated with care. Some boxes follow a feature of the cloud as it develops in time and a time series within a single box shows development within a specific area for a Lagrangian-like case.

The atmospheric properties were simply averaged over all 65 levels in the RAMS model and interpolated to the 54 layers of the laser transmission model. Figures 2.6, 2.7, and 2.8 show the averaged profiles of temperature, pressure, and water vapor mixing ratio respectively for one averaging box and time. For every box and time step examined, profiles like these were generated for the laser transmission model. The vertical averaging for the optical properties is described for each model in the sections below.

2.3.2 Single Layer Model

The 1-D model simply requires a cloud top height and a cloud bottom height and a single number for the each cloud property in between. The heights were calculated by taking an average cloud top and an average cloud bottom of air with a water relative humidity value of 85%. The cloud and any clear air contained within that level and contained in that averaging box was then included in the overall average of optical variables. Figure 2.9 shows a vertical schematic picture of the averaging layer.

2.3.3 Multiple Layer Model

The multi-layer model requires a cloud top and cloud bottom height with layer averages for all layers in between. The cloud top was calculated using the same 85% relative humidity criteria but by using an average cloud top and bottom value. The averages of the optical variables for all of the layers were then calculated. Figure 2.9 shows an example of this method. Any clear air found within the average top and bottom cloud layers was included in the averaging of the optical variables.
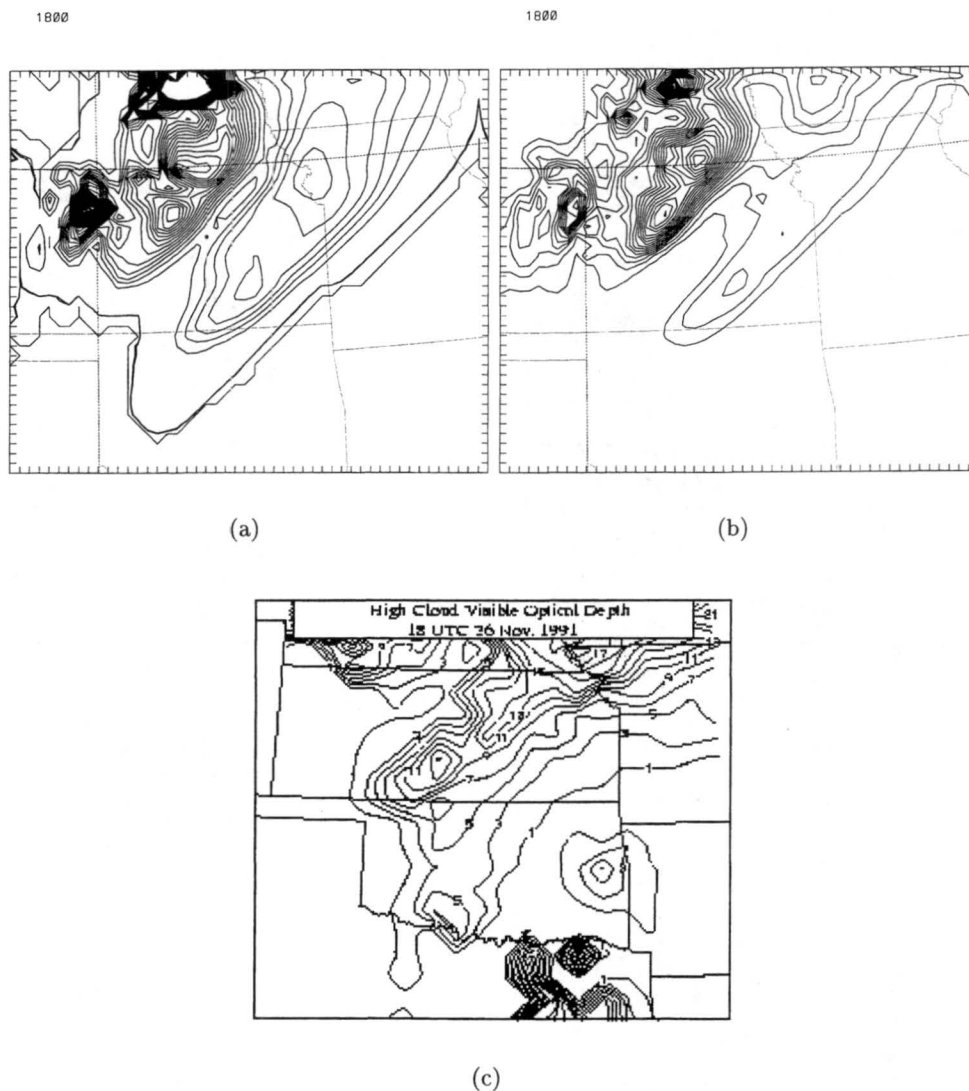
Figure 2.4: (a) Mesoscale model (grid 2) 7200 m above sea level total ice number concentration at 18 hours into the simulation at contour intervals of 5000 1/kg; (b) Mesoscale model (grid 2) cloud optical depth (solar band 3: 0.245-0.7 μm) computed from the two-stream radiation code at contour intervals of every 1 unit at the same time as (a); (c) high cloud visible optical depths derived from GOES data at 1800 UTC 26 November 1991, taken from Mace et al. (1995).

1700
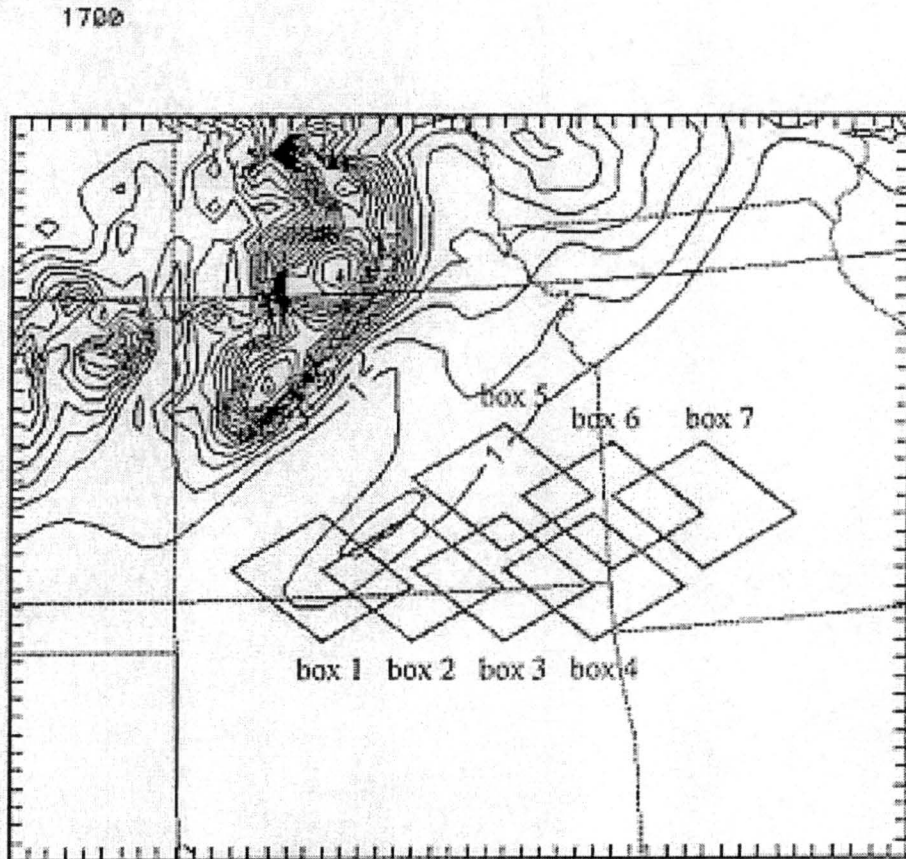
Figure 2.5: Single time plot of optical depth from grid 2 with the averaging boxes from 17 hours into the simulation. As time progresses, the cloud fills the boxes to the right of the domain.
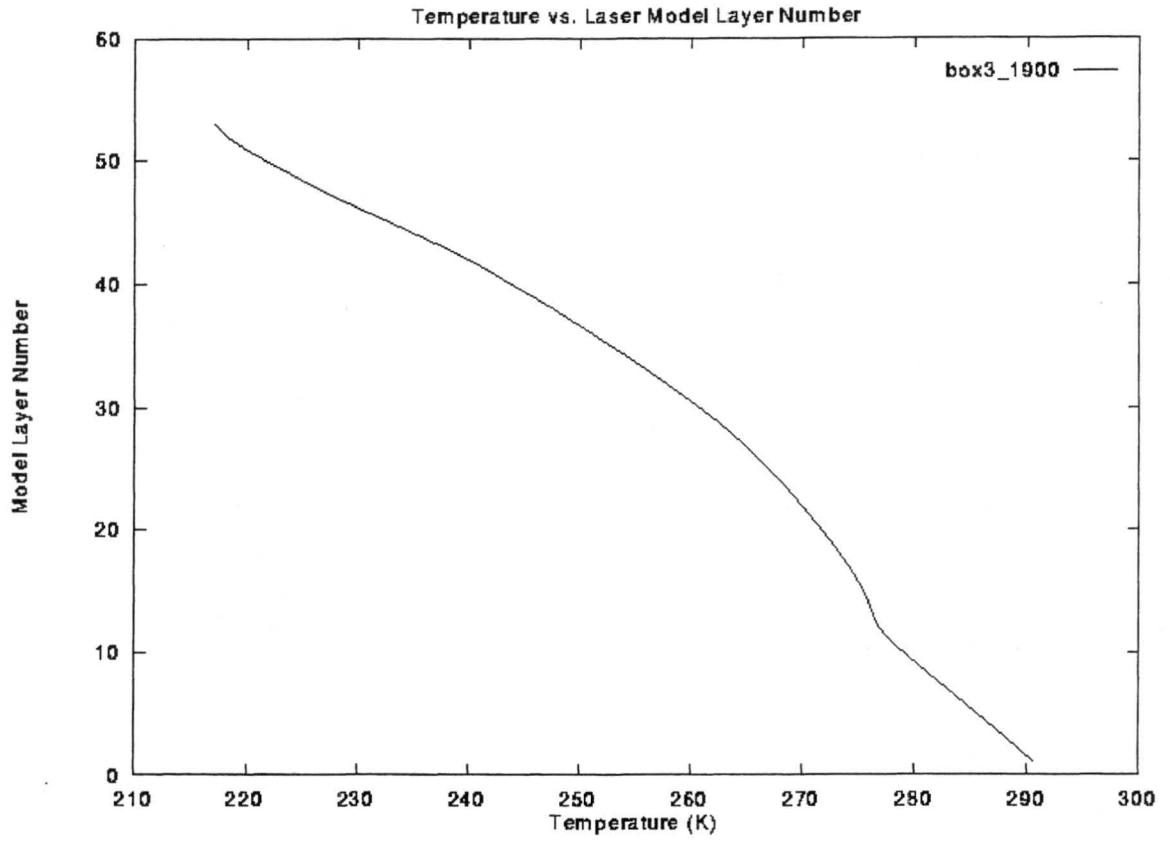
Figure 2.6: Profile of box averaged temperature from RAMS. Note that model layer number 0 corresponds to the surface and model layer number 53 corresponds to 13 km.
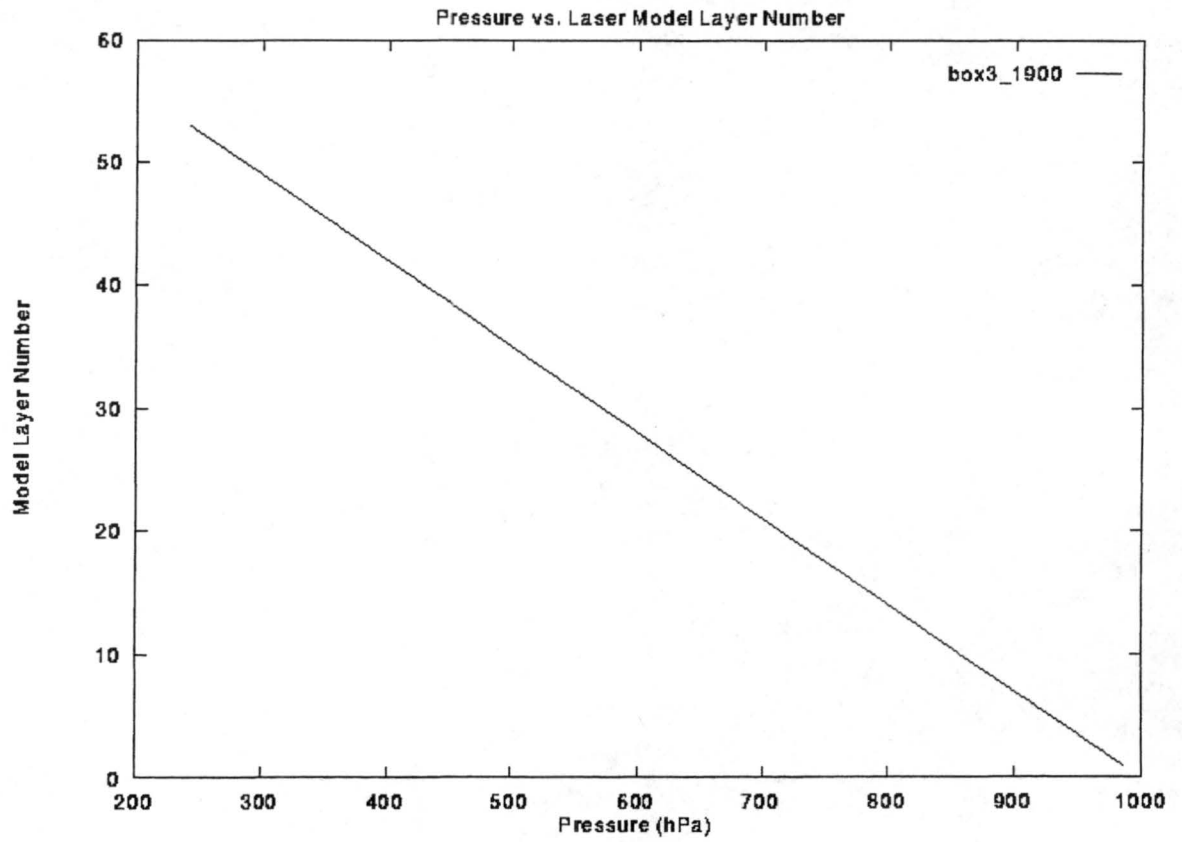
Figure 2.7: Profile of box averaged pressure from RAMS. Note that model layer number 0 corresponds to the surface and model layer number 53 corresponds to 13 km.
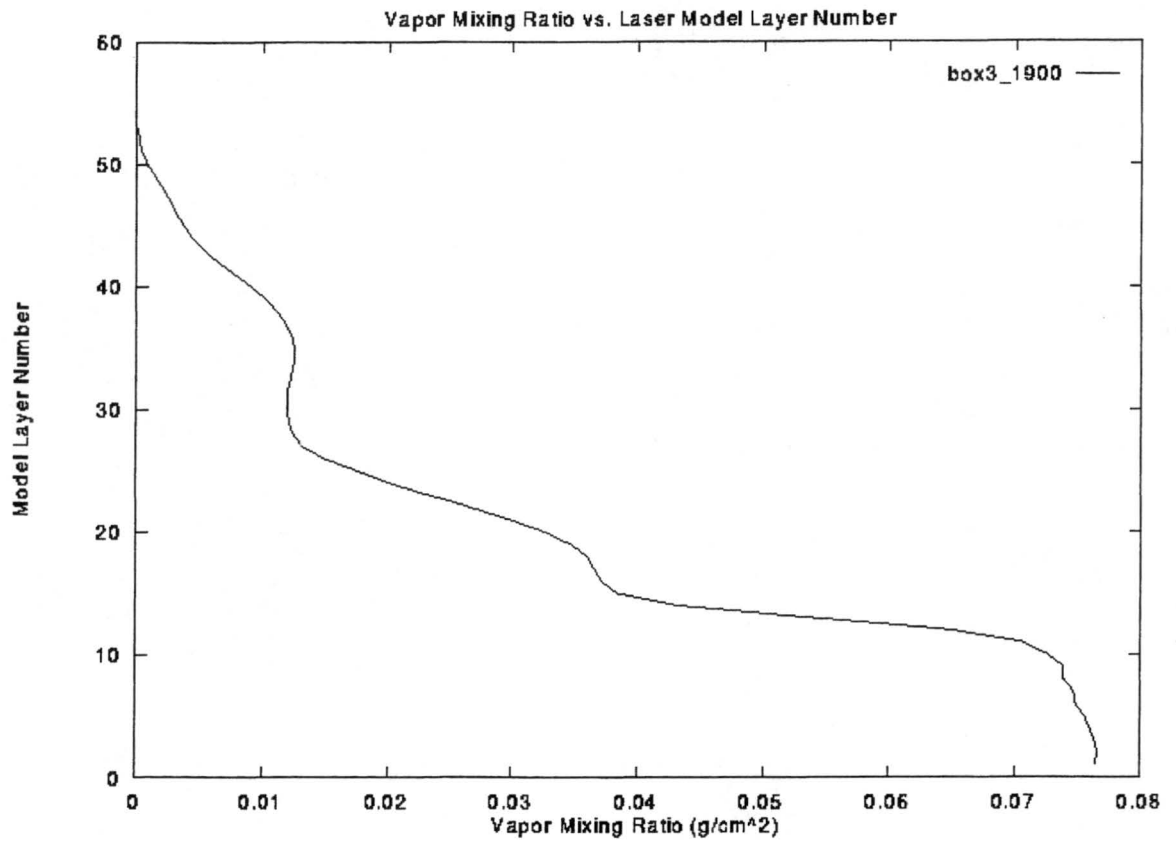
Figure 2.8: Profile of box averaged water vapor mixing ratio from RAMS. Note that model layer number 0 corresponds to the surface and model layer number 53 corresponds to 13 km.

Average Cloud Top

Height

Average Cloud Bottom

Horizontal Averaging Box

Average Cloud Top

Layer 4

Layer 3

Layer 2

Layer 1

Average Cloud Bottom

Height

Horizontal Averaging Box
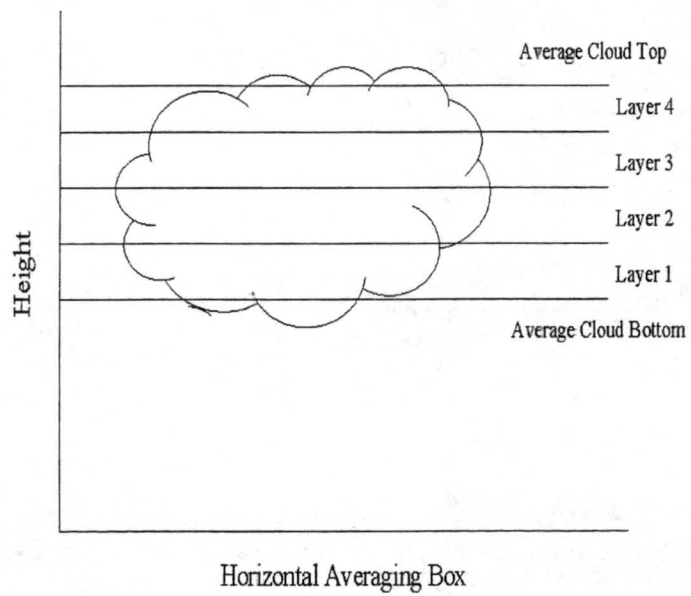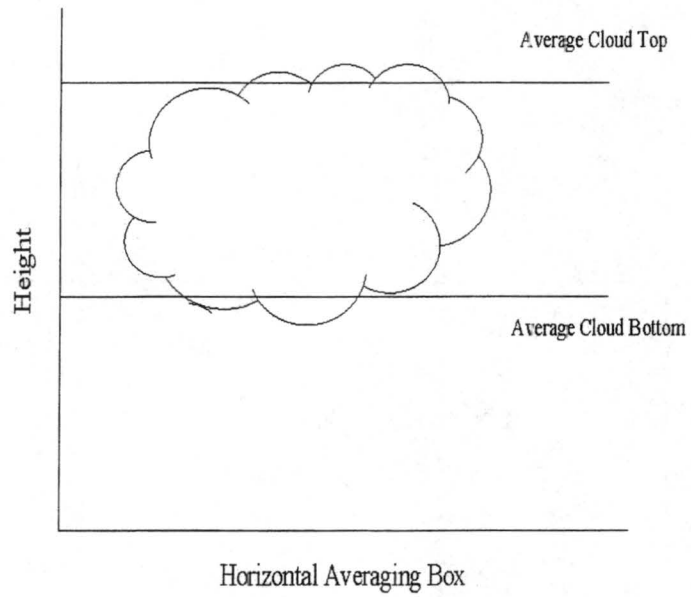
(b)

Figure 2.9: (a) Single layer vertical cross section within an averaging box and (b) multi-layer vertical cross section within the averaging box.

Chapter 3

THE LASER TRANSMISSION MODELS

3.1   Background

Liou et al. (1986, 1992, 2000) studied and developed transmission models for cirrus clouds over the past 15 years. Applications such as input to global climate models to extinction of laser beams have found use in such models. The Institute of Radiation and Remote Sensing (IRRS) at UCLA, under the direction of Dr. K. N. Liou, developed laser transmission models specially for long path laser transmission through high cirrus clouds. These models take into account ice crystals, air molecules, water vapor, and aerosols in the direct transmission formulation. They also account for multiple scattering contributions following Liou et al. (1990). These codes have been used to examine cases of cirrus uncinus, cirrostratus, cold cirrus, and contrail cirrus. Different conditions within a realistic simulated cloud case have not yet been examined.

3.2   Model Details

3.2.1   Formulation of Transmission

Direct transmission comes from the exponential of the attenuation. It can be written in terms of the transmitted power F_d:

$$F_d = F_0 exp(-\beta_e s) = F_0 exp[-(\beta_{air} + \beta_{aerosol} + \beta_{cloud} + k_v\rho)s], \qquad (3.1)$$

where F_0 is the laser power in units of Watts, the total extinction coefficient β_e, which is the sum of the scattering coefficient of air molecules, β_{air}, the extinction coefficient of

aerosols, $\beta_{aerosol}$, and cirrus clouds, β_{cloud}, and the absorption coefficient of water vapor multiplied by water vapor density, $k_v\rho$, and the parameter s which is the distance along the laser beam between the cloud top and cloud base.

Multiple scattering contributions follow the work of Liou et al. (1990). The transmission due to n-th order scattering $F^{(n)}(0, \Omega)$ is:

$$F^{(n)}(0, \Omega) = \int_0^s J^{(n)}(s', \Omega) exp(-\beta_e s')\beta_e ds', \qquad n = 1, 2, 3, ..., \qquad (3.2)$$

where the n-th order source function $J^{(n)}$ is defined by:

$$J^{(n)}(s', \Omega) = \frac{\omega}{4\pi} \int_{\Delta\Omega} F^{(n-1)}(s', \Omega) P(\Omega', \Omega) d\Omega', \qquad (3.3)$$

where $P(\Omega', \Omega)$ is the scattering phase function of the cloud particles and ω is the single scatter albedo. For this formulation, the laser beam is assumed to be collimated, so no angular width is included in the equation. The term s' is a distance along the laser beam between the cloud base and a certain point in the cloud. Therefore the transmission due to the first order scattering can be expressed:

$$F^{(1)}(0, \Omega) = exp[-(\beta_{nc,a}\nu + \beta_{nc,b}u)] \int_0^s J^{(1)}(s', \Omega) exp(-\beta_e s')\beta_e ds'. \qquad (3.4)$$

Exponential attenuation outside of the cloud is accounted for in Equation 3.4 and $\beta_{nc,a}$ and $\beta_{nc,b}$ are the extinction coefficients due to non-cloud materials (air molecules, aerosols, and water vapor) above and below the cloud respectively, u represents the distance from the cloud base to the surface, and ν is a distance between the laser platform and the cloud top.

The second order scattering is developed in Liou et al. (2000) and is expressed:

$$F^{(2)}(0, \Omega') = exp[-(\beta_{nc,a}\nu + \beta_{nc,b}s_3)] \int_0^s J^{(2)}(s", \Omega') exp(-\beta_e s_2)\beta_e ds", \qquad (3.5)$$

where s" is the position where second order scattering occurs along the path and s_2 and s_3 are relevant angles to the cloud and the target.

3.2.2 Scattering and Absorption Parameters

Calculating laser transmission through a cloudy and clear atmosphere requires single scattering and absorption parameters for ice crystals, aerosols, and water vapor related to the specific laser wavelength used.

3.2.3 Ice Crystals

Takano and Liou (1995) developed a series of light scattering models for crystals of various shapes and sizes. Using a Monte-Carlo/geometric-ray-tracing method, the scattering, absorption, and polarization properties for large ice particles with several structures including solid and hollow columns, single and double plates, dendrites, bullet rosettes, and aggregates are computed. The details of this technique can be found in Takano and Liou (1989, 1995) and Liou et al. (2000)

The refractive indices for ice for a given laser wavelength are interpolated from Liou (1992). Based on observed ice crystal habit and size distributions of typical cirrus clouds, the ice crystal model consists of a combination of 50% bullet rosettes/aggregates, 30% hollow columns, and 20% plates. Table 3.1 shows the values of the complex refractive indices for ice used in the model.

3.2.4 Air Molecules

The extinction coefficient of air molecules is calculated as parameterized by Hansen and Travis (1974):

$$\beta_{air} = \frac{\tau_{air}}{\Delta z} = 0.008569\lambda^{-4}(1 + 0.0113\lambda^{-2} + 0.00013\lambda^{-4})\frac{\Delta p}{\Delta z p_0}, \tag{3.6}$$

where Δz is the thickness of a layer whose pressure difference is Δp, λ is the laser wavelength, and p_0 is the surface pressure, 1013.25 hPa (Liou et al. 2000).

3.2.5   Aerosols

The extinction coefficient of aerosol, $\beta_{aerosol}$, is defined by using the standard aerosol (IHAZE=1) of MODTRAN3.7 (Anderson et al. 1995) due to the fine resolution of the size distribution as a function of altitude. Figure 3.1 shows the US1976 standard atmospheric profile and the extinction coefficient for standard aerosol. There is a cloud layer present between 9 - 9.5 km which can be seen by the higher relative humidity within that layer. This atmospheric profile was used by Liou et al. (1999 and 2000). The majority of the aerosols are located below 4 km, below the cloud layer. By interpolating the extinction coefficient, single scatter albedo, and asymmetry factor to the wavelength of interest from d'Almeida et al. (1991) the single scatter properties of aerosol are computed and are listed in Table 3.1.
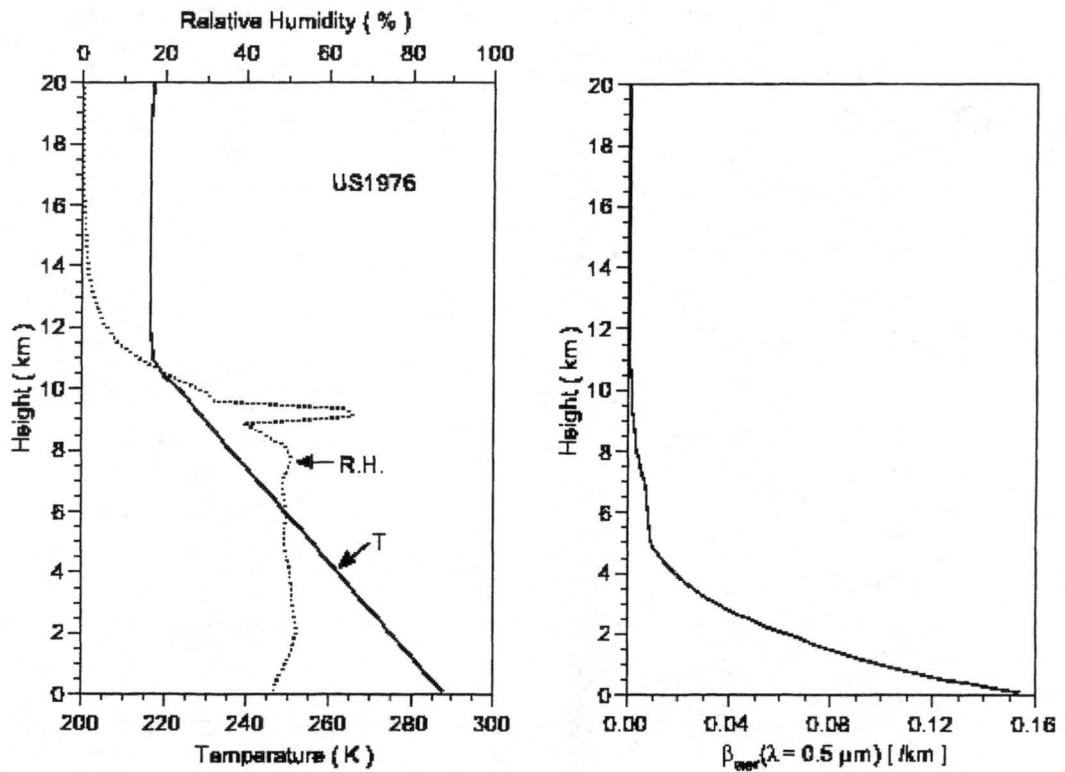
Figure 3.1: Atmospheric profile and extinction coefficient for aerosols assumed in the laser transmission computation, from Liou et al. 1999.

Table 3.1: Parameters for ice crystals and rural aerosols at a laser wavelength of 1.315 μm.

	Wavelength 1.315 μm
Refractive index m_r	1.2957
Complex refractive index m_i	1.3150E-5
β_e	0.2703
ω	0.8365
Asymmetry factor	0.6252

3.2.6 Water Vapor

Absorption by water vapor is handled by using the correlated k-distribution method. In this method, the wavenumber integration is transformed into an integration over the cumulative probability which is a monotonically increasing function in absorption coefficient space (Fu and Liou 1992). The correlated k-distribution method has been used to obtain the absorption coefficient of water vapor based on the HITRAN92 line by line database (Rothman et al 1992). Absorption from water vapor is incorporated into the scattering calculations by adjusting the extinction coefficient and the single scattering albedo associated with cloud and aerosol particles (Liou et al. 2000).

3.2.7 Required Input

For each scenario of cirrus cloud and platform-target geometry, the transmission model requires certain input. Geometric variables such as laser platform height, laser to target horizontal distance, cloud top and bottom height and layer number, as well as cloud and atmospheric parameters, such as single scatter albedo, transmission, extinction, and profiles of temperature, relative humidity, pressure, and vapor mixing ratio, are needed. A given background profile of aerosols is assumed for this work, from Figure 3.1.

The model is able to calculate the transmission for a variety of platform-target geometries to include a vertical profile of the transmitted power at each of the 54 layers in the model to an angled sweep through the cloud layer. Figure 3.2 shows an example of an angled sweep geometry with the laser platform located above the cloud layer. Note that
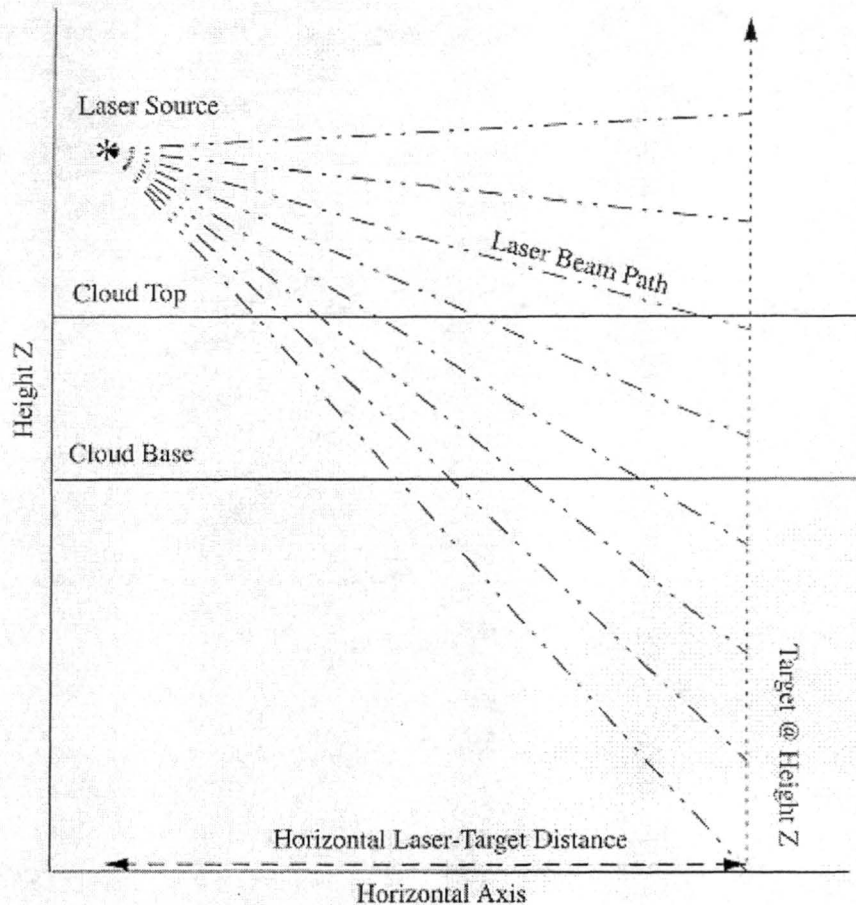
Figure 3.2: Description of a typical angle sweep laser-target geometry. Note that as the target increases in altitude below the cloud layer the path length of the beam within the cloud grows. This would be expected to cause an decrease in transmission as more cloud is in the way of the target.

the beam path within the cloud increases as the height of the target below the cloud layer also increases, thus intercepting more cloudy air than when the target is at the surface. For a straight vertical geometry this will not occur.

This transmission model is very flexible and able to account for different cloud scenarios, atmospheric profiles, laser properties, and platform-target geometries. With such flexibility, it is possible to tailor this model for a variety of applications from optical communication to laser ranging.

3.3 Single Layer and Multiple Layer Models

The transmission model described above is still in development. The first generation of this model used a simple homogeneous cloud layer that the laser beam would be shot through. Though using a single homogeneous layer seems simple, the model is still calculating second order scattering and contributions from aerosols, air molecules, and water vapor. The second generation model uses multiple layers to incorporate vertical variations within the cloud. Optical properties and layer heights are given for each layer within the 54 model layers that contain cloud.

3.3.1 Single Layer Model

This model calculates the transmission through, within, and above a single homogeneous 1-D cloud layer. No cloud variation is accounted for and the cirrus cloud is generalized to one set of numbers for single scatter albedo, transmission, and extinction. This requires any cirrus data to be averaged to that one set of numbers and a great deal of resolution is lost. Horizontal as well as vertical variations are gone and the cloud is generalized most by the method used to average the cloud properties from the simulation or observations.

3.3.2 Multiple Layer Model

The addition of accepting some vertical variations within the model layers is the second step in the laser transmission model's development. Clouds clearly vary in the vertical and cirrus often occur in layers. This model accounts for vertical inhomogeneities for clouds that span over more than one of the model layers. This code requires input of the optical properties for each layer containing cloud. This model is still averaging a great deal of the possible resolution offered by cloud models such as RAMS but it does include possible vertical variations within clouds spanning over more than one model layer.

3.3.3 Future Models

These two models are the first and second steps to making a fairly accurate laser transmission model. The next step will be to accept coarse gridded data in the horizontal domain and add more vertical levels to increase the vertical resolution. More resolution in the horizontal will bring about a very realistic model and the limit will be the resolution of observations and/or model simulations. This will take time to incorporate and these models will soon be available as they are developed. The multiple layer model offers a worst case scenario at the very least and is useful to help determine threshold values for laser operators.

Chapter 4

LASER TRANSMISSION MODEL SENSITIVITY TESTS

The laser transmission models have a great deal of flexibility in terms of what is included in the calculation and how the transmission scenario is set up. Table 4.1 shows the parameters that can be changed within the laser models and need to be set for each scenario. The sensitivity of certain options within the model are examined, such as horizontal vs. random orientation of ice crystals, inclusion of water vapor and aerosols to the model vs. without aerosols and water vapor, and multiple scattering vs. single scattering. These tests will justify the method used in examining all of the cloud data.

Sensitivity of the laser transmission models to differences in laser wavelength were not performed. Since the size of the ice crystals are large enough that the extinction coefficient approaches the value 2, the transmission values will be nearly wavelength independent. Appendix B discusses this in more detail.

Table 4.1: Variables to be set for each scenario for the laser transmission code input.

	Units or Mode
Laser Wavelength	μm
Horizontal Laser Target Distance	km
Diameter of Laser Beam	m
Laser Power	W
Laser Altitude	km
Aerosol Flag	on/off
Water Vapor Flag	on/off
Second Order Scattering Flag	on/off
Horizontal Orientation Flag	on/off
Horizontal Plate Orientation Flag	on/off

4.1   Ice Crystal Orientation

The spatial orientation of ice crystals within a cloud has a significant impact on light scattering and radiative transfer within the cloud. According to Jayaweera and Mason (1965) freely falling cylinders in a viscous fluid will fall with their long axes horizontal if the ratio of diameter to length is less than one. Ono (1969) observed natural clouds and discovered that columnar and plate crystals fall with their major axes oriented horizontally. Platt et al. (1978) showed that cirrus clouds at approximately -15° C contain mostly plates oriented horizontally. Since there is some experimental and observed evidence that ice crystals may be predominantly oriented in the horizontal, that situation should be examined.

The laser transmission models have a flag for choosing random ice crystal orientation or horizontal orientation. Takano and Liou (1989b) show that when plates are oriented horizontally, as opposed to randomly in the atmosphere, they reflect more solar flux with the exception of when the sun is directly overhead. In that case the transmission in the greatest. Liou et al. (2000) showed that for thin clouds, with optical depths of 0.05 and 0.2, the horizontal plate orientation gave the highest transmission with the 3-D horizontal orientation giving the lowest, with the random or Parry orientation being in between. Therefore, it would be expected that the horizontal orientation would make the clouds less opaque to the laser beam.

Figure 4.1 shows 3 cases from averaging box 2, an optically thin cloud with average optical depth of 1.1 at time step 1700, a cloud which is of moderate optical depth with average optical depth of 1.3 at time step 2100, and an optically thick case with average optical depth 4.3 at time step 2300. Each time step was run with the exact same model set up for the single layer model with only the ice crystal orientation flag being different. The lines labeled horizbox2 were run with horizontal orientation and the lines labeled box 2 were run with random orientation of ice crystals.

The cases with the horizontal orientation clearly have more transmission than the cases with the randomly oriented ice crystals. The difference seems to be greatest for the
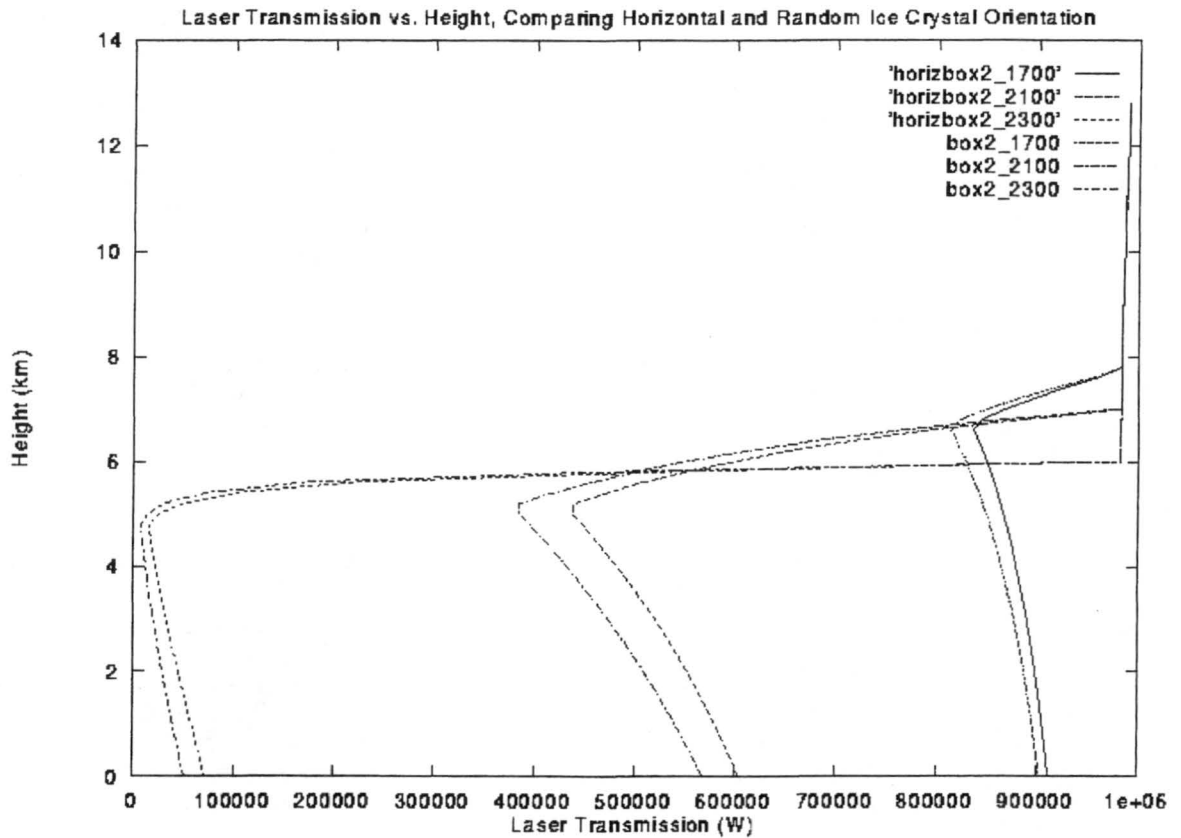
Figure 4.1: Plot of three times from box 2 with the horizbox2 lines representing the transmission model run with all ice crystals oriented horizontally and the box2 lines representing randomly oriented ice crystals.

2100 time step where the cloud depth is fairly thick; about 2 km. The other cases have a cloud depth of about 1 km and show a smaller difference. The difference for the 2100 time step is 53,028 W and this could be enough power to meet a given threshold for a laser system. Due to fairly large difference and the difficulty of knowing the exact orientation of ice crystals in any given cloud, a random orientation of ice crystals is used in this work to offer a worst case scenario.

4.2 Water Vapor and Aerosols

Including water vapor and aerosols in the transmission calculation would cause an expected decrease in the transmitted power in the lower levels where aerosol and water vapor mixing ratios are highest. Above the cloud layer the effect of atmospheric aerosols is still significant until about 6 km where the aerosol profile drops off, as seen from Figure 3.1.

Water vapor is found throughout the model atmosphere with the majority of it found in the cloud filled layer and will effect the transmission at all levels. It is very clear that water vapor has a large effect on the transmission at many levels in the atmosphere.

Figure 4.2 shows the same three cases from the previous example with both the aerosol and water vapor contributions included for the aerobox2 lines and without those contributions for the box2 lines. It is clearly seen that the addition of water vapor and aerosols have a strong effect on the lower atmospheric transmission and has some effect above the cloud layer. The curves seem to match again at about 12 km where water vapor and aerosols are scarce. This corresponds well with the results from Liou et al. (2000).

The addition of aerosols and water vapor has the greatest affect on the thinner (depth) clouds, the clouds at 1700 and 2100 in the simulation. Not only is the transmission below the cloud level effected but the minimum transmission values are also much smaller. For realistic scenarios, these effects are very strong and must be taken into account. For this work however, the focus is to isolate what the effect of cirrus clouds are and therefore the additional effects of aerosols and water vapor are neglected.

4.3 Single and Multiple Scattering Effects

The second order scattering calculation uses a great deal of computer time and could be neglected if the contribution is small as suggested by Liou et al. (2000). For very small optical depths, it was shown that the first order scattering had an effect on the order of 10^3 while the second order scattering was on the order of 10^{-4}. For higher optical depths
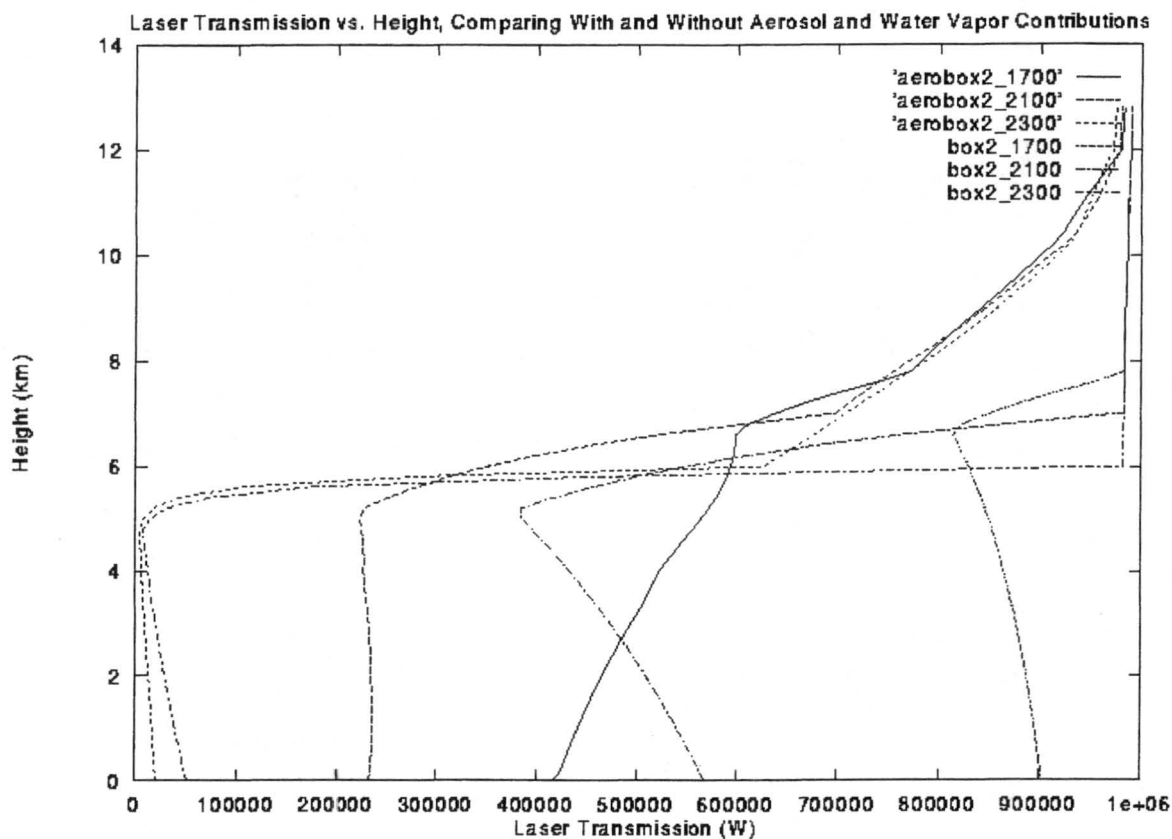
Figure 4.2: Plot of three times from box 2 with the aerobox2 lines representing the transmission model run including aerosol and water vapor contributions and the box2 lines representing no aerosol and water vapor contributions.

the first order scattering was still high on the order of 10^2 while second order scattering contributed the same amount. In both cases from Liou et al. (2000) the second order scattering was negligible.

Figures 4.3, 4.4, and 4.5 show the same three cases as before showing the direct transmission, first order scattering contributions, and the second order scattering contributions respectively. The first order scattering contributions basically follow that the larger the transmission the smaller the scattering. The second order scattering, however, shows something a little different. The 2100 case shows the highest contribution from second order scattering. This could be due to the thickness of the cloud layer. This cloud is

about twice as thick as the other two cases offering more occasion for light to be scattered. Though this amount is significantly larger that the other shown cases, it is still very small and can be neglected. Figure 4.6 shows the direct transmission for those same three cases against the transmission including the scattering. It is clear from these results that for this scenario, the scattering contributions are minimal. For a scenario with a wider beam, such as a satellite-based laser, (this work used a 1.5 m beam diameter) the scattering contributions could be more important and should be examined.
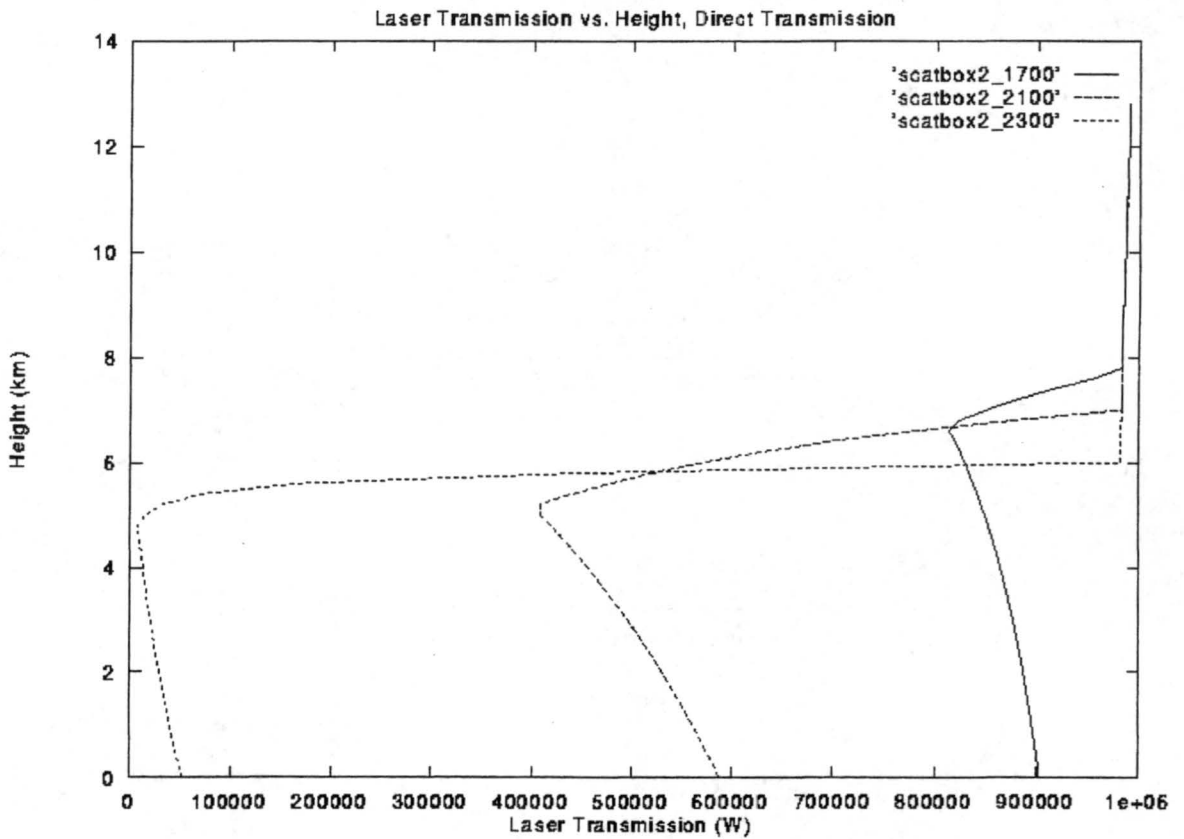
Figure 4.3: Plot of three times from box 2 of the direct transmission.
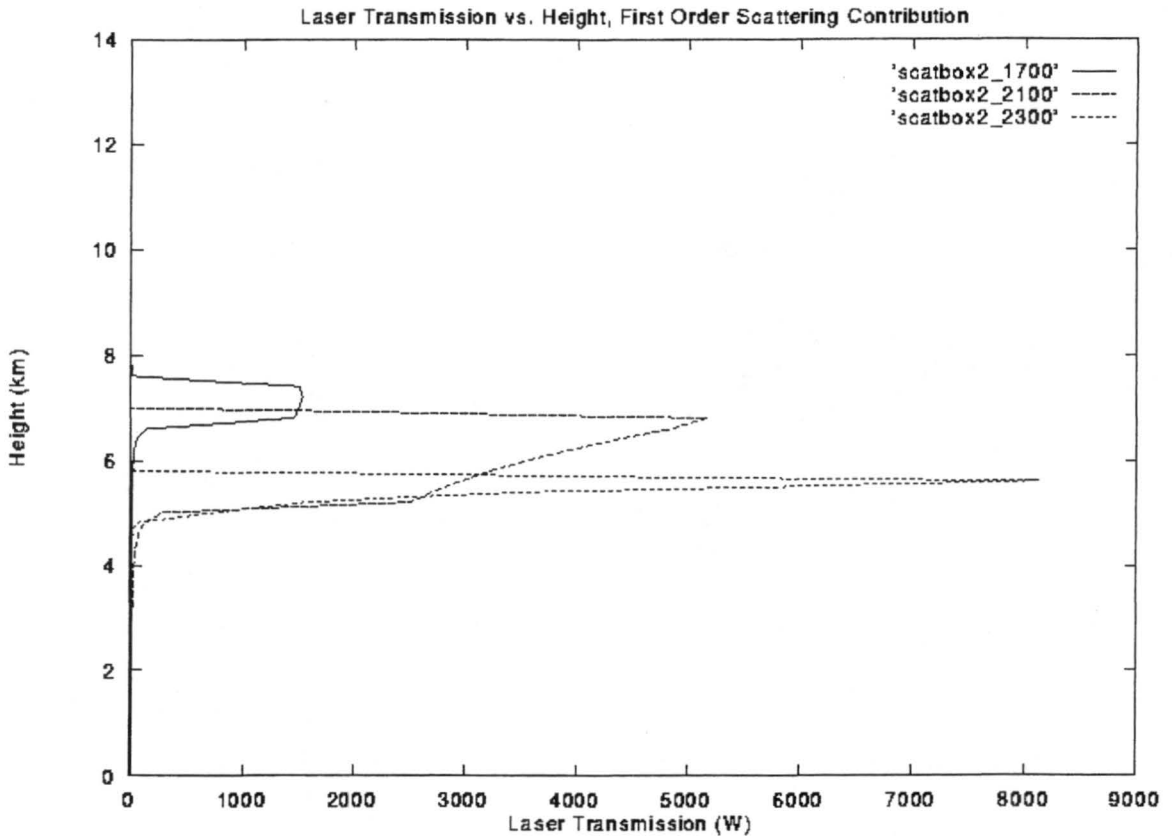
Figure 4.4: Plot of three times from box 2 of the first order scattering contribution to the transmission.

4.4 Summary

The laser transmission models are clearly sensitive to these additional effects that are options to the model. Since the purpose of this work is to examine the effects of cirrus clouds on laser transmission, it makes sense to make the laser transmission model set up to isolate those effects. Since cirrus clouds are dynamic, consistent orientation of all the ice crystals within the cloud seems unlikely for extended periods of time. Certainly there could be a majority of the crystals horizontally-oriented in any given cloud but the model assumes all the crystals are horizontally-oriented. This could dramatically underestimate the transmission for a cloud that contained even half of the crystals not
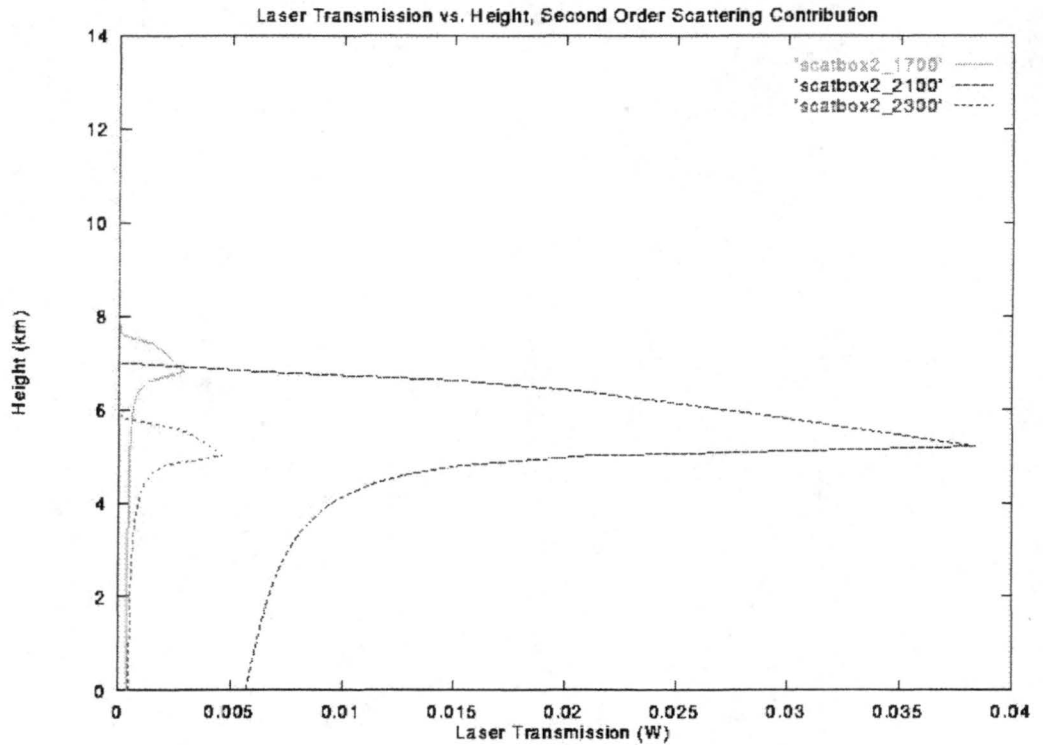
Figure 4.5: Plot of three times from box 2 of the second order scattering contribution to the transmission.

horizontally oriented. For this reason, random orientation of ice crystals is chosen. A random orientation offers a worst case scenario that would be more conservative than assuming any homogeneous orientation. The second order scattering seems to offer a very small contribution to the direct transmisssion values as shown in Liou et al. (2000). Given a different scenario, perhaps a wider laser beam, the second order scattering would offer more of a contribution and would need to be included in the analysis.

These sensitivity tests offer a concept of the best way to run the models to obtain the effects of realistic cirrus clouds on laser transmission. The next chapter examines the results of running both laser models, the single layer and the multi-layer, on different parts of the cirrus case.
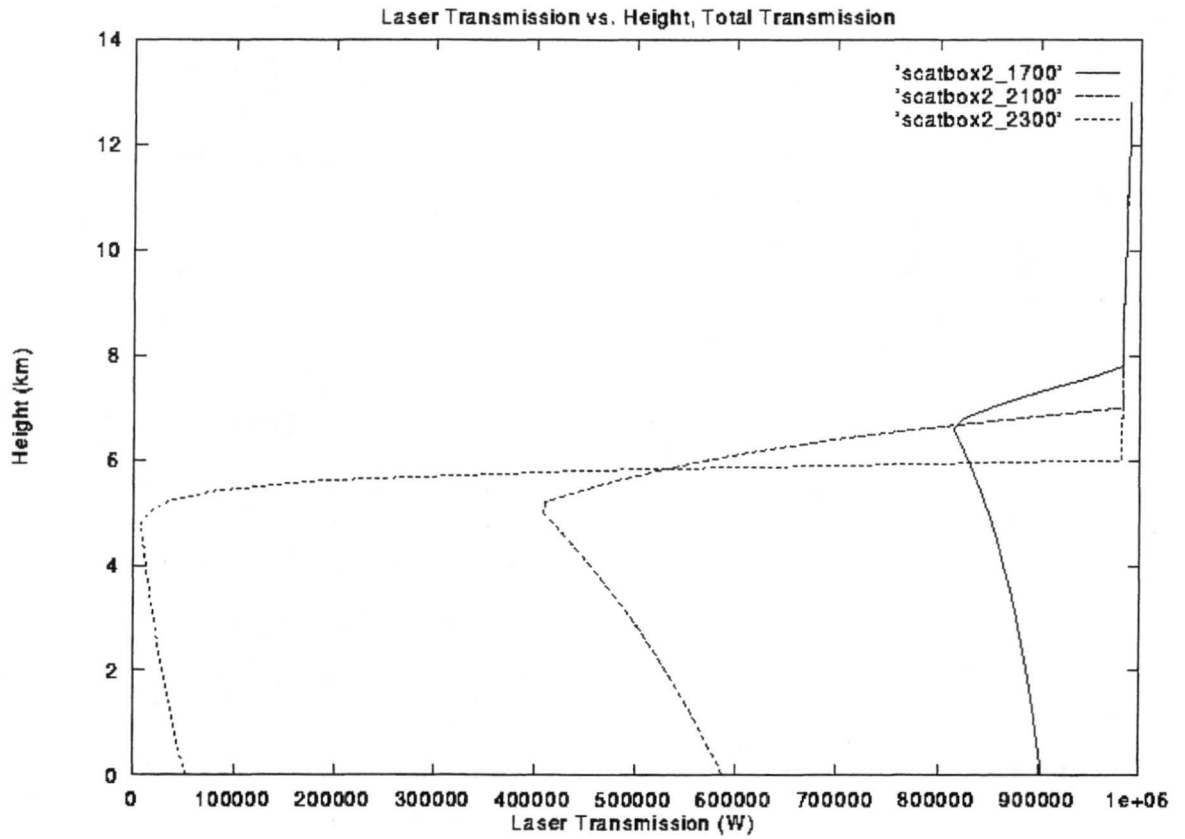
Figure 4.6: Plot of three times from box 2 of both scattering contributions and the direct transmission.

Chapter 5

LASER TRANSMISSION MODEL RESULTS

5.1 Method

After reviewing the sensistivity of the laser transmission model, the entirety of the cloud data within the averaging boxes were examined using a single model set up and a single laser-target geometry. The model set up is listed in Table 5.1.

Table 5.1: Values for the chosen scenario for the laser transmission code input.

	Value
Laser Wavelength	1.315 μm
Horizontal Laser Target Distance	100 km
Diameter of Laser Beam	1.5 m
Laser Power	1.0×10^6 W
Laser Altitude	12 km
Aerosol Flag	off
Water Vapor Flag	off
Second Order Scattering Flag	off
Horizontal Orientation Flag	off
Horizontal Plate Orientation Flag	off

This set up examines a vertical sweep through the horizontal cloud layer and could be typical for an airborne laser platform and a target at any of the model's 54 levels. The wavelength of the laser is chosen since it is within one of the atmospheric window regions. Figure 5.1 shows a plot of the absorptivity of selected gases in the atmosphere and the total atmosphere. Note the log scale of wavelength. The high laser power is chosen to offer a large range to examine the cloud's effect on the transmission. The aerosol and water vapor flags were turned off to isolate the cirrus cloud contribution. The second order scattering was also turned off since the contribution was small and to minimize computer

time. The ice crystal orientation was chosen as random to offer a worst case and perhaps be a more generic scenario.
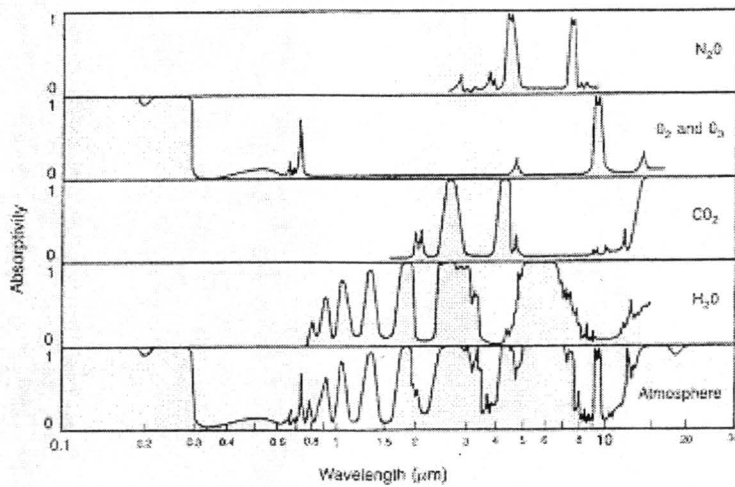
Figure 5.1: The absorptivity of select gases in the atmosphere and the total atmosphere. (From Lutgens et al. 1992)

All 7 averaging boxes at all 9 time steps were examined with both the single layer model and the multiple layer model. The time steps of averaging boxes that contained no cloud or that the transmission was completely saturated are not plotted on the transmission graphs. The simulated cloud data were examined for each averaging box through time and for a series of averaging boxes following a particular feature over time. Figure 5.2 shows the boxes overlaid on optical depth plots that follow the band of interest over the times examined. After all the data are examined, an optical depth vs. transmission plot was generated including both models to offer insight into when the optical depth of a cloud may be too strong to penetrate.

5.2 Single Layer Model Results

Averaging box 1, averaging box 3, and averaging box 7 offer a varied look at laser transmission as the cloud moves through the box with time. The other boxes showed similar results with more profiles attenuating the laser completely. The averaging boxes

(a) 1700 (b) 1800 (c) 1900

(d) 2000 (e) 2100 (f) 2200
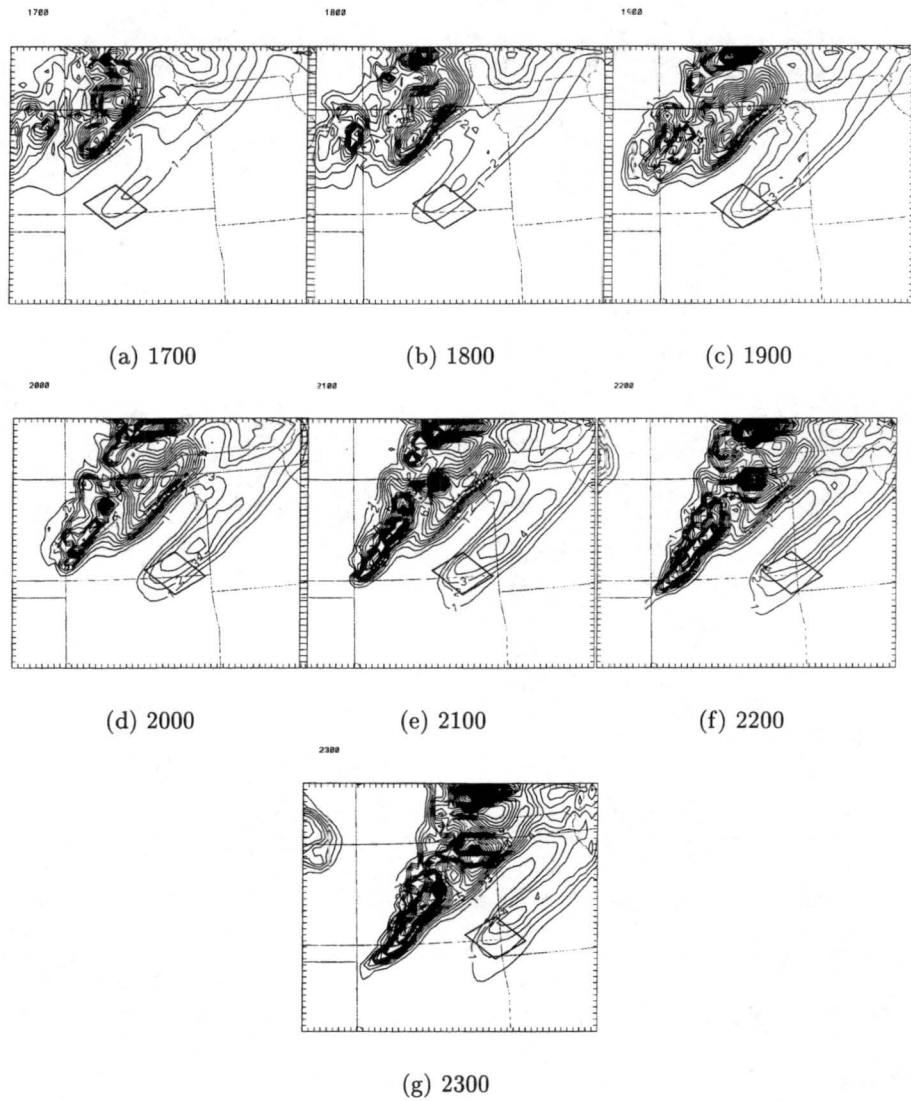
(g) 2300

Figure 5.2: RAMS generated optical depth plots with band following averaging boxes from (a) 1700; (b) 1800; (c) 1900; (d) 2000; (e) 2100; (f) 2200; and (g) 2300 into the model run.

following a developing band showed that as the optical depth increases in the band, the cloud becomes more opaque until no laser power is transmitted below the cloud.

5.2.1 Time Series

Figures 5.3, 5.4, and 5.5 show the time series progression for averaging boxes 1, 3, and 7 respectively. These plots show the laser transmission against the target height for a single averaging box for each cloud time step. Features to note on these plots are: the steady decrease of transmission from a value at the surface to the base of the cloud, the

steady increase of transmission through the cloud layer, and the value approaching full power at the top of the cloud layer up. The steady decrease of transmission from the surface is due to the geometry of the scenario. Figure 3.2 shows that as the target height increases below the cloud level, the path length within the cloud layer increases until the target reaches the base of the cloud layer. For a straight vertical geometry, this decrease would not exist. The increase within the cloud level is due to the beam path within the cloud becoming shorter and shorter until the target is above the cloud layer when the only effect reducing transmission would be air molecules.
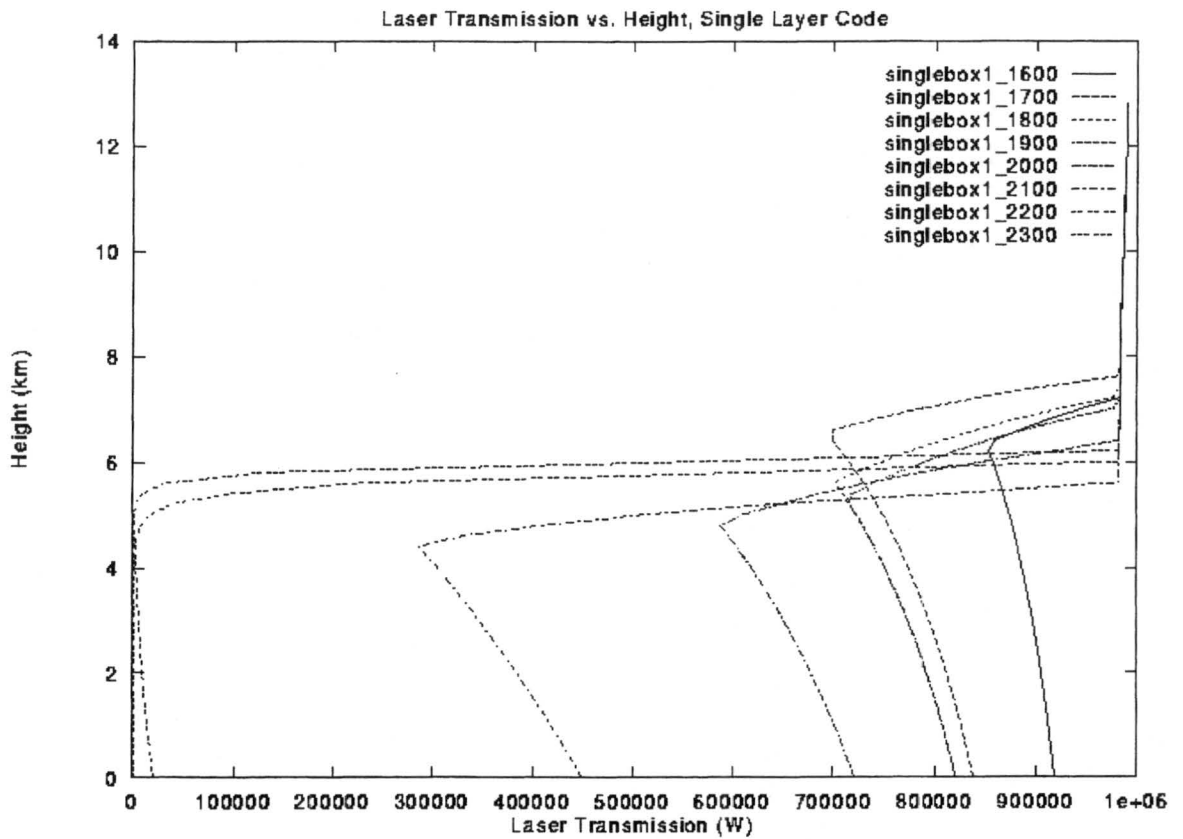
Figure 5.3: Laser Transmission vs. Target Height for a time series within a particular averaging box, box 1 for the single layer model.

For box 1, the average optical depth ranges from 0.54 at 1600 to 7.0 at 2300. Optical depth seems to be a fairly good measure of how well the laser beam will be transmitted
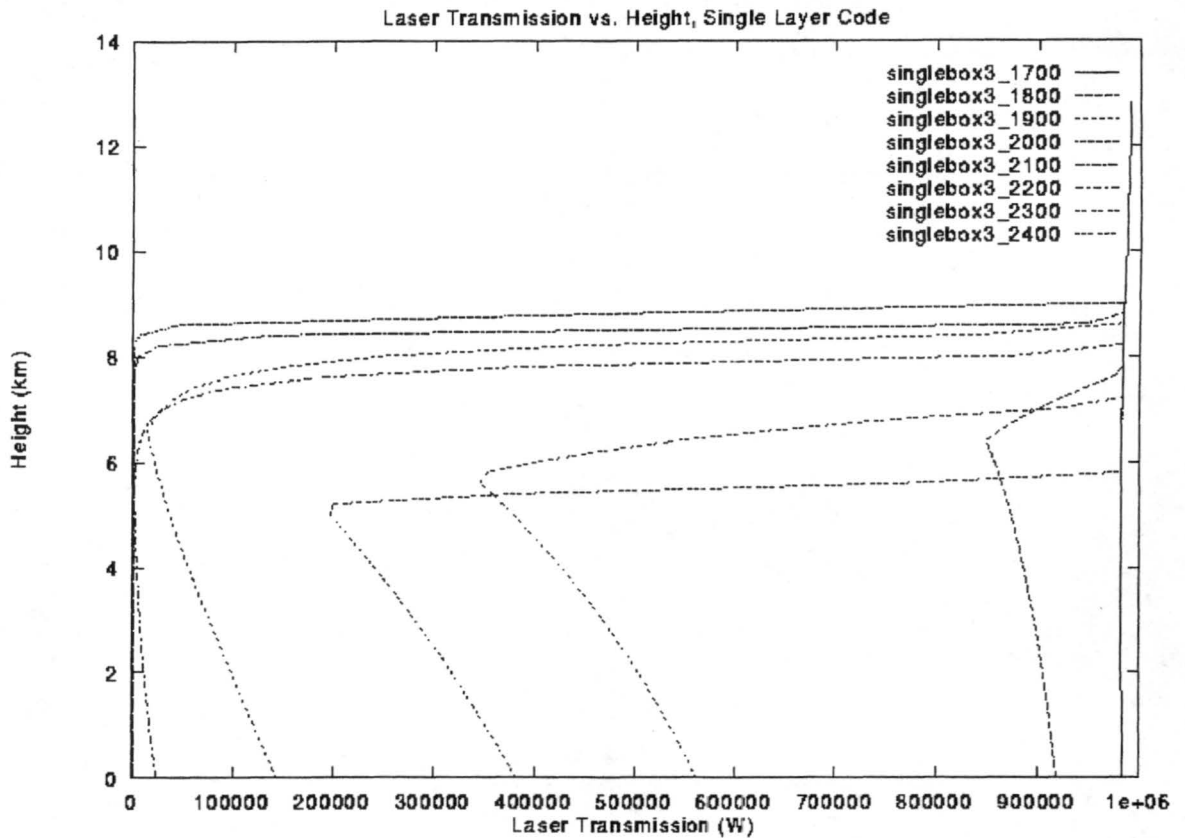
Figure 5.4: Laser Transmission vs. Target Height for a time series within a particular averaging box, box 3 for the single layer model.

and is a derivable quantity from satellite information. It is not perfect since size distribution and number concentration can also have an impact on the transmitted power. However, those quantities are more difficult to quantify without taking cloud samples of the particular cloud of interest. For box 1, the times that have optical depths of 1.5 or less are found to reduce the transmission by less than half while the times with optical depths above 1.5 reduce the transmission by more than half to almost completely. Box 3 shows similar results with the optical depth threshold even lower for half of the transmitted power to make it through to the base of the cloud layer at 1.1. Box 7 showed some slightly different results with an optical depth of 4 allowing about half of the transmitted
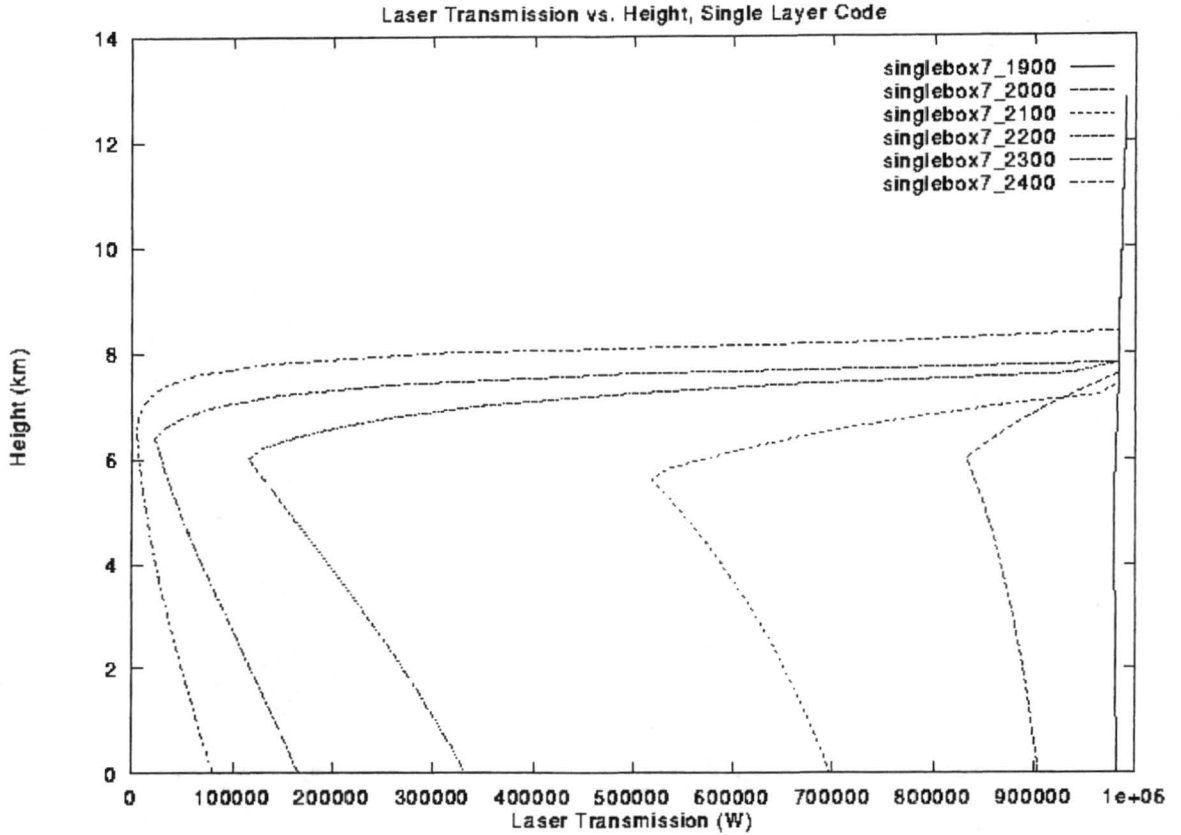
Figure 5.5: Laser Transmission vs. Target Height for a time series within a particular averaging box, box 7 for the single layer model.

power through. Table 5.2 shows the minimum transmission values with the corresponding time and average optical depth value.

5.2.2 Band Progression

The boxes that follow a particular band within the simulation are put together to create a plot of the transmission through a developing cloud band, as seen in Figure 5.6. The same features as in the time series are found on this plot. The average optical depth of the first curve, which allows some power to be transmitted below the cloud layer, is 0.928. The values of average optical depth for the other curves, which allow little to no transmission, range from 1.5 to 2.6. It is also fairly clear to see from Figure 5.2 that

Table 5.2: Values of optical depth and minimum transmitted power at each time step for boxes 1, 3, and 7 from the single layer transmission model.

Time step	Optical Depth	Transmission (W)
Box 1		
1600	0.542	8.525×10^5
1700	0.928	6.984×10^5
1800	1.555	7.012×10^5
1900	1.142	7.154×10^5
2000	0.581	5.868×10^5
2100	1.544	2.861×10^5
2200	6.111	2.199×10^3
2300	7.023	3.609×10^1
Box 3		
1700	0.268	9.810×10^5
1800	1.181	8.482×10^5
1900	2.156	1.443×10^{-2}
2000	2.614	4.212×10^{-2}
2100	2.616	2.506×10^{-1}
2200	2.215	1.194×10^3
2300	1.354	3.570×10^5
2400	1.219	1.961×10^5
Box 7		
1900	0.576	9.783×10^5
2000	1.908	8.316×10^5
2100	4.001	5.175×10^5
2200	4.678	1.142×10^5
2300	3.804	2.224×10^4

the optical depth increases with time which would be expected to reduce the transmitted power reaching the surface.
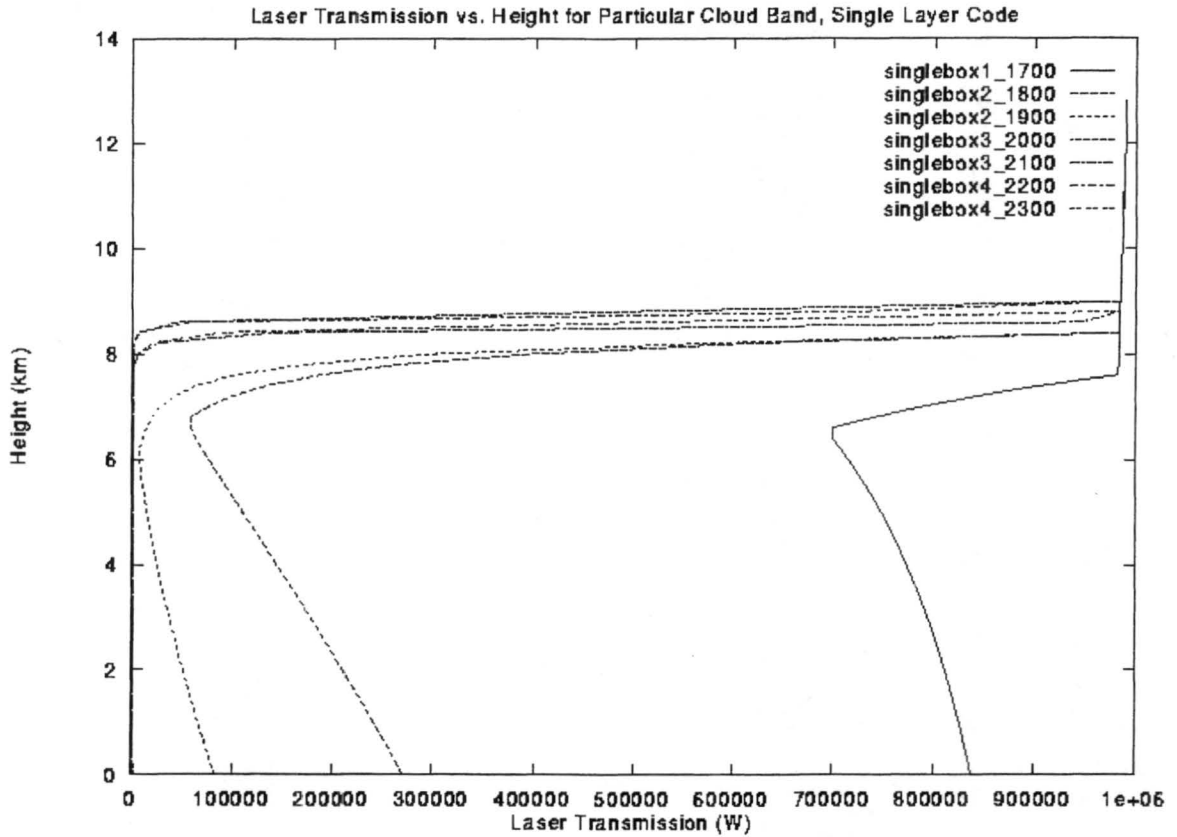
Figure 5.6: Plot of laser transmission for a particular cloud band through time from the single layer model.

5.3 Multiple Layer Model Results

The results from the multiple layer model are very similar to those of the single layer model, with the multiple layer model offering slightly more transmission through the cloud layer in some cases. Since cirrus clouds often have a vertically-banded structure, this model attempts to capture some of the vertical structure that is simulated in the RAMS model output. The same cases of the time series for averaging boxes 1, 3, 7 and the band progression are examined.

5.3.1 Time Series

The time series for boxes 1, 3, and 7 are shown in Figures 5.7, 5.8, and 5.9 respectively. The same features are seen as in the single layer model results: the decrease in transmission from the surface to the cloud base, the strong increase within the cloud layer, and the gradual increase from the top of the cloud to full power.
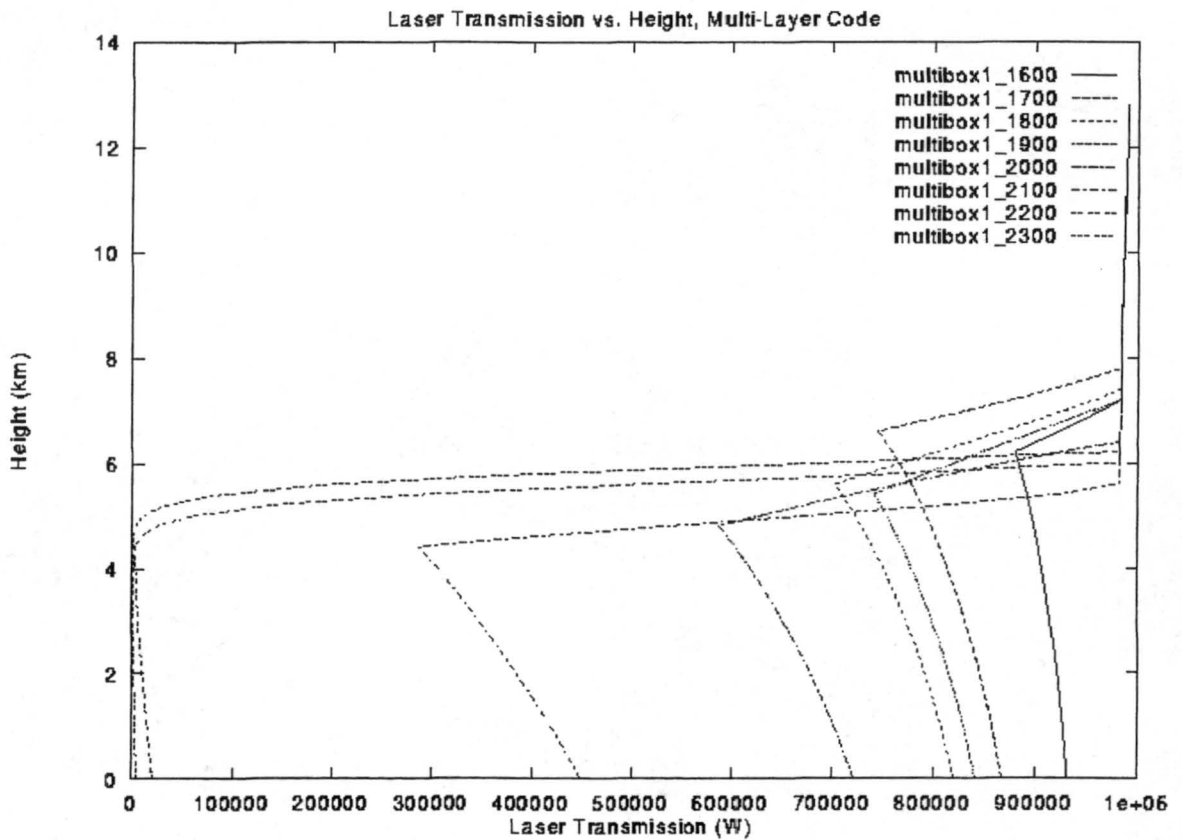

Figure 5.7: Laser Transmission vs. Target Height for a time series within a particular averaging box, box 1 from the multi-layer transmission model.

These results are similar to the single layer model with a few exceptions. The results of averaging box 1 are very similar to that of the single layer model with more than half of the transmitted power reaching the cloud base for average optical depth values of 1.5 and less. Values for times 1600, 1700, and 1900 show the largest difference between the
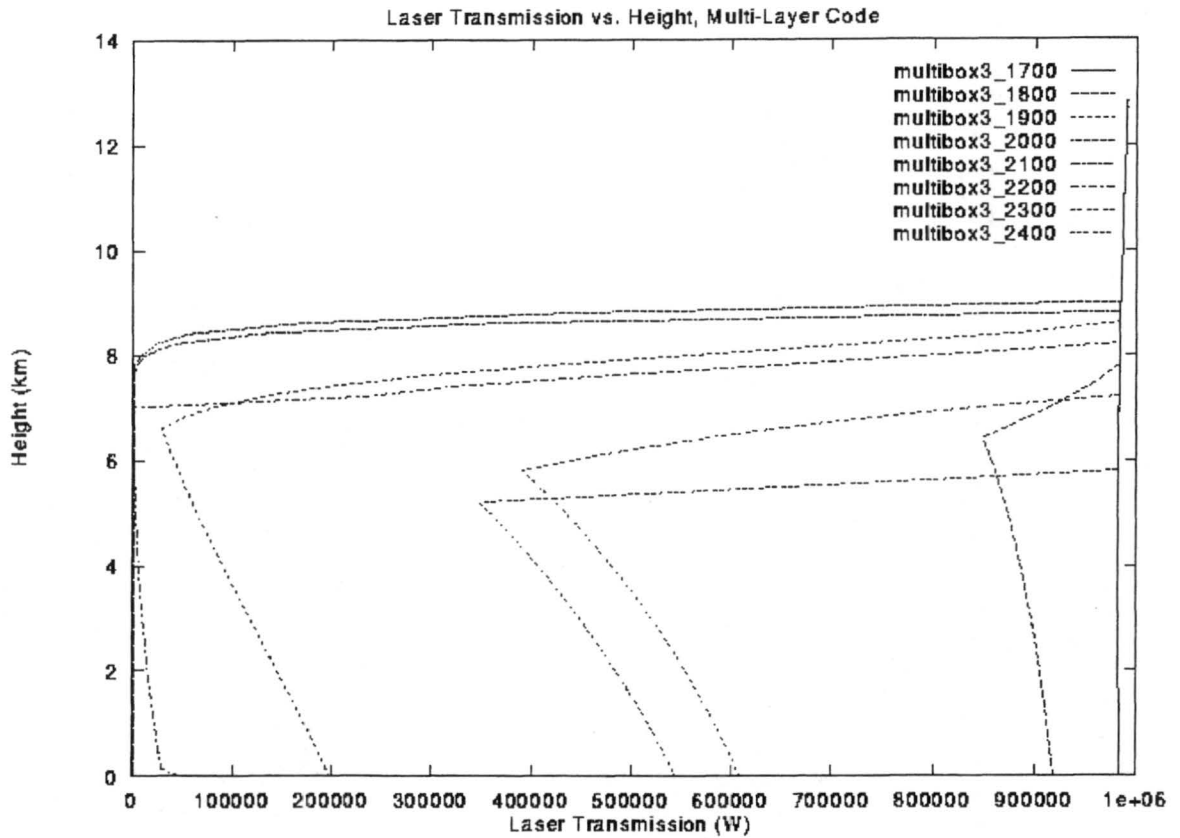
Figure 5.8: Laser Transmission vs. Target Height for a time series within a particular averaging box, box 3 from the multi-layer transmission model.

two models with the multi-layer code resulting in higher transmission values. The other time steps show little to no difference at all with only the shape at the cloud base as the transmission increases above it is sharper for the multi-layer model. This is most likely due to the way the multi-layer model handles the inhomogeneity between the cloud layers.

The average optical depth threshold for box 3 to transmit at least half of the laser power is still found at 1.1. Box 3 shows very similar results to the single layer model with the multi-layer model offering more transmission for time steps 1900, 2300, and 2400. Again the other time steps have the same transmission minima as the single layer code with just the slight shape difference at the cloud base.
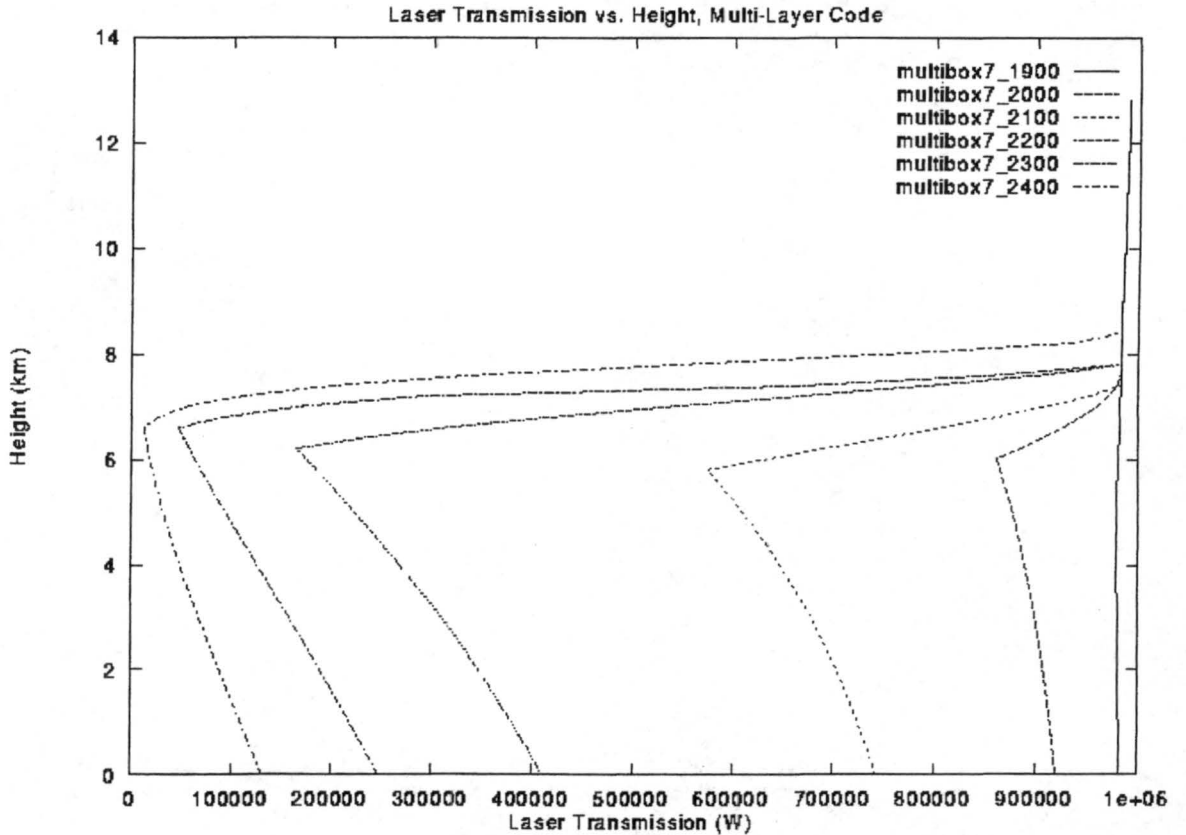
Figure 5.9: Laser Transmission vs. Target Height for a time series within a particular averaging box, box 7 from the multi-layer transmission model.

Box 7 again shows a slightly better picture than the other averaging boxes with the average optical depth allowing half of the transmitted power to reach the bottom of the cloud at 4.0. Box 7 shows higher transmission for all the cases for the multi-layer code than the single layer code, with varying degrees. Table 5.3 show the optical depth and minimal transmission values for each case plotted.

5.3.2 Band Progression

The cloud band followed is the same as in the single layer case. Figure 5.10 shows the plots of laser transmission against target height for the band case run with the multi-layer model. The first averaging box in the progression, with an average optical depth of 0.928,

Table 5.3: Values of optical depth and minimum transmitted power at each time step for boxes 1, 3, and 7 from the multiple layer transmission model.

Time step	Optical Depth	Transmission (W)
Box 1		
1600	0.542	8.796×10^5
1700	0.928	7.444×10^5
1800	1.555	7.012×10^5
1900	1.142	7.409×10^5
2000	0.581	5.868×10^5
2100	1.544	2.865×10^5
2200	6.111	2.254×10^3
2300	7.023	1.749×10^2
Box 3		
1700	0.268	9.811×10^5
1800	1.181	8.481×10^5
1900	2.156	2.853×10^4
2000	2.614	7.280×10^{-4}
2100	2.616	4.297×10^{-4}
2200	2.215	2.276×10^2
2300	1.354	3.901×10^5
2400	1.219	3.478×10^5
Box 7		
1900	0.576	9.783×10^5
2000	1.908	8.601×10^5
2100	4.001	5.729×10^5
2200	4.678	1.639×10^5
2300	3.804	4.664×10^4

is the only one which allows any significant amount of power through the cloud layer. The other time steps, which have average optical depths ranging from 1.50 to 2.99, allow little to no transmission. The only main difference with the multi-layer model in this case is the first time step of box 1 at 1700, where the single layer model has a transmission value of $6.985 \text{X} 10^5$ W and the multi-layer model has a value of $7.444 \text{X} 10^5$ W, a difference of 45,500 W. This could be the difference between a successful laser penetration and a failed one. The model differences are important and should be examined further.
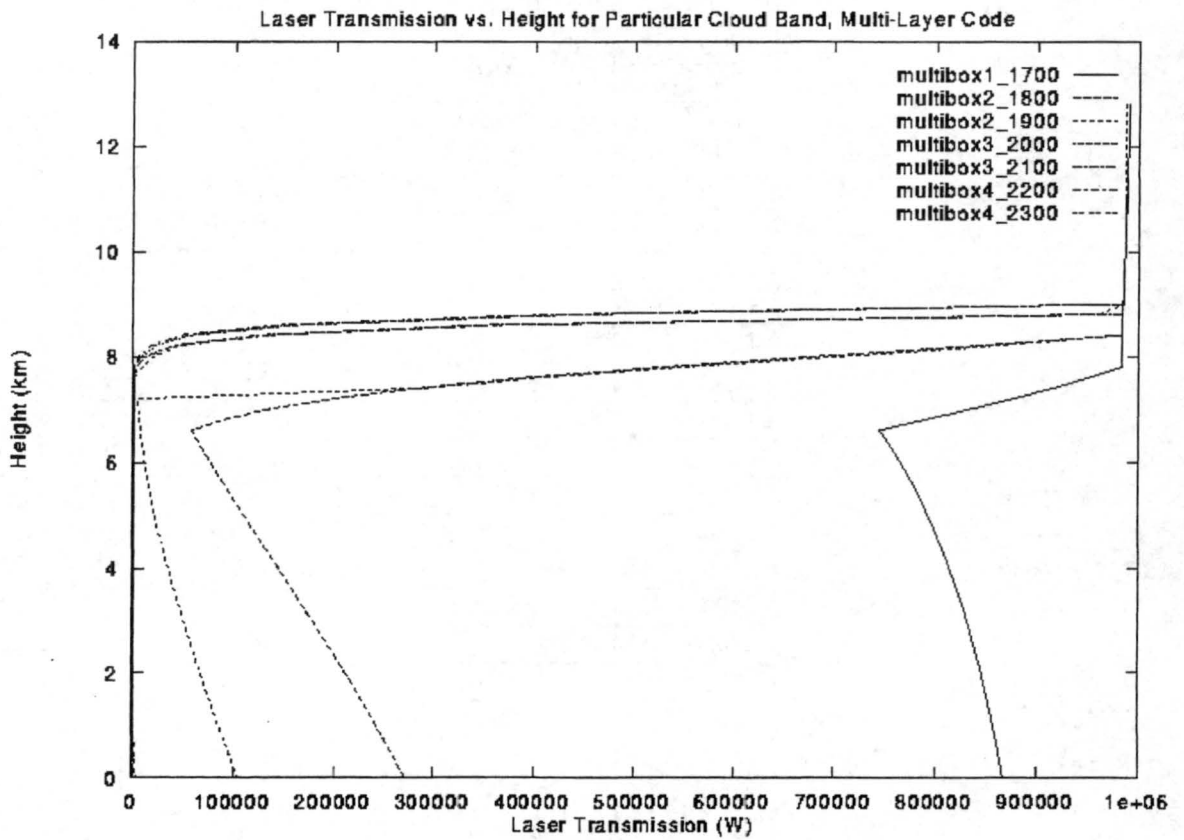

Figure 5.10: Plot of laser transmission for a particular cloud band through time from the multi-layer model.

5.4   Single and Multi-layer Model Comparison

The single layer model and multi-layer model clearly show differences in the trans-mitted laser power in the cloud cases examined. The difference ranges from little or no difference in transmitted power to as much as 50,000 W. Depending on the threshold of the laser system being used, that difference could be the deciding factor between sys-tem success or failure. By examining the differences between the single layer model and the multi-layer model it is possible to determine what difference is caused by the models themselves and what is due to the actual cloud vertical variations.

Figure 5.11 shows a model comparison for one averaging box within the case study. The Multi-Layer Data line represents the multi-layer model output from the multi-layer model with multiple cloud layer average input from the RAMS model. The Single-Layer 1-D Data line represents single layer model output from the the single cloud layer average input. The Multi-Layer 1-D Data line represents the multi-layer model output with a single layer average input for all layers. It is to be expected that these curves will not be the same since the models handle the data differently.

The multi-layer model incorporates the effects of vertical inhomogeneity of the cloud and therefore offers a slightly different output from the single layer model, even when the input numbers are the same. The difference between the single layer model and the multi-layer model with multiple layer data is very clear, on the order of 30,000 W for this example. Vertical variations do indeed make a difference in the transmitted power. This could be enough of a difference between a successful and unsuccessful operation. The single layer model is useful for providing a "worst case scenario" but the multi-layer model offers a more realistic scenario if the cloud data are available.

5.5   Optical Depth vs. Transmission

All of the cloud averaging boxes for each time step offer a varied distribution of data points that can offer a picture of what optical depth threshold will allow the desired amount of power through a cloud layer. Figure 5.12 shows a scatter plot of every data point

run for both the single layer (crosses) and multi-layer (diamonds) models. From this figure it is very obvious how the multi-layer model consistently has higher transmission values than the single layer model. About half of the values are the same but none of the multi-layer values have lower transmission. There are clearly more effects than just variations in optical depth causing laser extinction but optical depth is the quantity most readily available from satellite information. Other variables such as ice crystal size distribution, number density, and depth of the cloud layer will also affect the amount of transmitted laser power. These quantities, however, are not readily available and are rapidly changing as a cloud develops.

From Figure 5.12 it is clear that there are a few points that seem to be outliers. Three points that have average optical depth values of 3.5 and higher offer transmission values 4.5×10^4 to 5.7×10^5. These points must have something different about them to have such high optical depths and allow so much power through. These three cases all occur within averaging box 7. The case that allows the most transmission contains about one half of clear air within the averaging box while the second most transmission has about one third clear air within the transmission box. The fact that the high optical depths offer such high transmission could be caused by averaging errors by including clear air in the cloud averaging. The depth of the cloud layer should not make any difference in the transmission values since the angle of incidence and the optical depth of the layer are the same. Table 5.4 shows some other average properties of these unusual cases and Table 5.5 shows similar optical depth values with more typical transmission properties for some of the cases.

Table 5.4: Values of optical depth, average cloud height, cloud layer depth, and transmission for cases with unusually high transmission. From the multi-layer model.

Box 7	Average Optical Depth	Average Cloud Height	Cloud Layer Depth (km)	Minimum Transmitted Power (W)	Percent Clear Air (%)
Case 2000	1.91	6.7	1.4	8.316×10^5	20
Case 2100	4.00	6.4	1.6	5.729×10^5	50
Case 2200	4.68	6.9	1.8	1.639×10^5	75
Case 2300	3.80	7.1	1.4	4.664×10^4	95

Table 5.5: Values of optical depth, average cloud height, cloud layer depth, and transmission for cases with typical transmission. From the multi-layer model.

	Average Optical Depth	Average Cloud Height	Cloud Layer Depth (km)	Minimum Transmitted Power (W)	Percent Clear Air (%)
Box 2 Case 1900	1.90	7.2	2.2	3.768×10^3	95
Box 6 Case 2100	4.02	7.1	2.2	2.576×10^2	100
No similar case	4.68				
Box 6 Case 2300	3.72	7.1	2.6	2.247×10^{-3}	75

As can be seen from the data in these tables, the clouds that are thicker have lower transmission values as well as the clouds that have more clear air within the box. It also seems that the higher clouds are more opaque. That, however, could just be an artifact of the deeper clouds extending higher into the atmosphere. Clearly the amount of clear air within the box for this averaging scheme must be taken into consideration as well as the optical depth when examining the transmissive properties. An averaging scheme wich does not include clear air in the calculations of optical properties will not have these errors.

Optical depth of a cloud can be determined by a number of ways using remote sensing techniques. The most widely used method is to use the GOES satellite data to determine cloud optical depth. This method is used in Mace et al. (1995) for the 26 November 1991 case, Figure 2.4, and described in Minnis et al. (1993). Methods using Advanced Very High Resolution Radiometer (AVHRR) data to retrieve cirrus cloud optical depth have been examined by Stone et al. (1990) and Ou et al. (1995). These techniques may not offer real time optical depth measurements but they can be computed fairly quickly. Mean ice crystal diameter can also be derived from AVHRR data as seen in Ou et al. (1995). Perhaps the future will offer real time optical depth information on all clouds captured by the GOES satellites.

With cloud optical depth information and optical depth vs transmission profiles for various different cases of cirrus, including tropical cirrus, cirrus uncinus, cirrostratus, Arctic cirrus, and contrail cirrus, it is possible to provide a laser system planner or operator with enough information to determine the viability of using the laser below the cloud level.
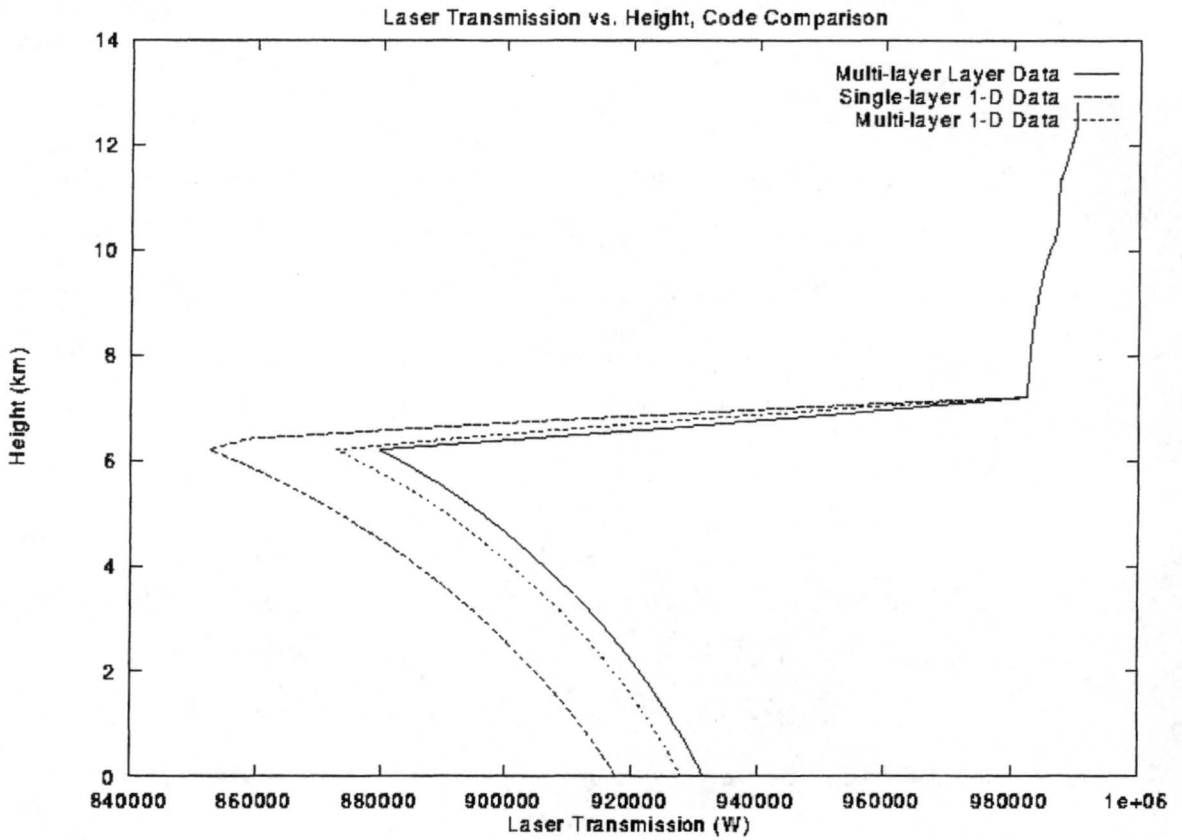
Figure 5.11: Comparison of the single layer and multi-layer models. The solid line represents the result from one averaging box at one time using the multi-layer model, the long dashed line represents the single layer model and the short dashed line represents the multi-layer model with the same average value, from the single layer model, for all cloud layers.
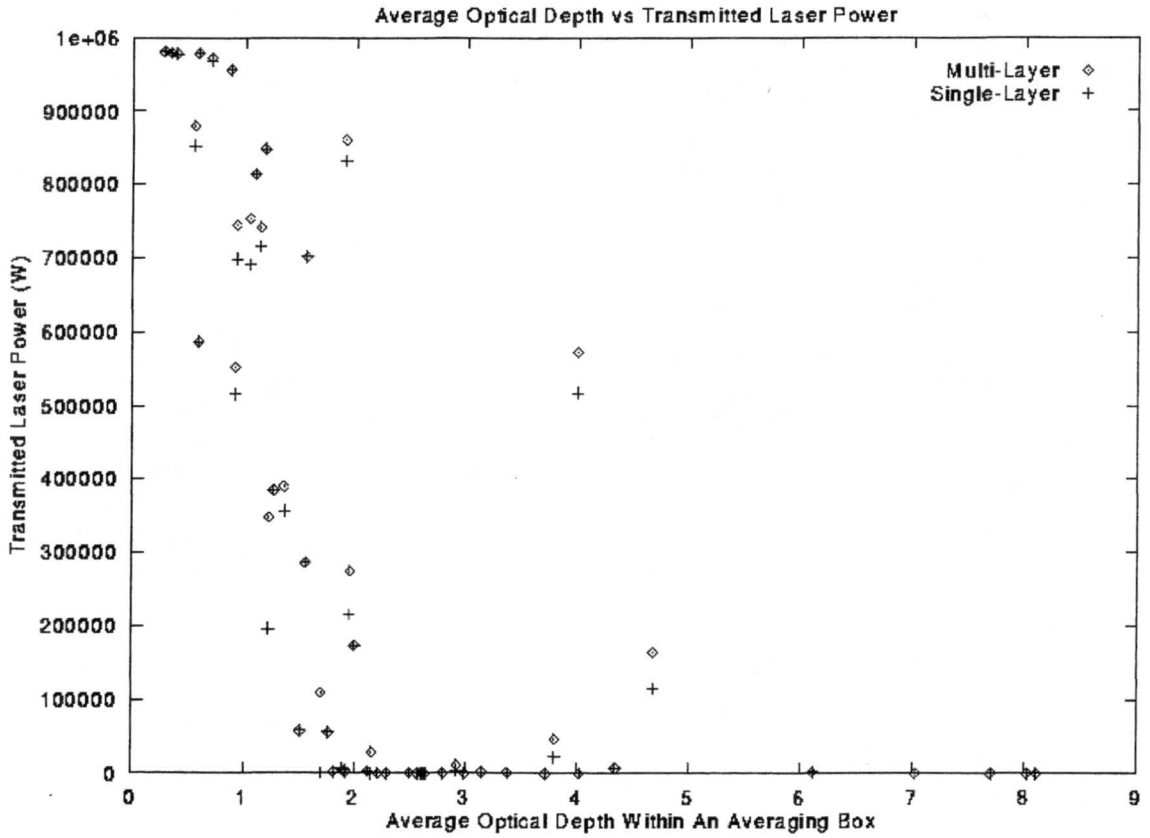
Figure 5.12: Scatter plot of laser transmission against optical depth from both the single and multi-layer models. This plot offers a quick reference to see at what optical depth will a transmission threshold be reached.

Chapter 6

SUMMARY AND CONCLUSIONS

6.1 Summary

A RAMS-generated thin cirrus cloud case is used as input to a single layer and a multiple layer laser transmission model. A simulation of a case from the FIRE Cirrus II field experiment is used to offer a realistic cloud case for the transmission model. The cloud information is averaged over large areas to fit into the laser transmission models. These models assume either a single homogeneous cloud layer, for the single layer model, or a series of homogeneous cloud layers to transmit laser power through. They provide the laser transmitted power in Watts for each given target height. They are able to account for extinction due to air molecules, aerosols, water vapor, as well as ice crystals of various shapes. The models can accomodate a variety of different laser target geometries to include vertical, horizontal, and sweeping beam paths. Laser transmission contributions due to ice crystal orientation, aerosols and water vapor, and second order scattering are examined for optically thin, moderate, and thick clouds.

All seven averaging boxes for each of the nine time steps of the cirrus cloud case are run through both the single and multiple layer models. The minimum transmission value for each box and time step is compared with the average optical depth. Optical depth provides an easy way to quantify clouds and their transmission properties. Remote sensing of cloud optical depth is possible through the use of various satellite instruments and therefore makes optical depth a measurable quantity that could be known prior to using a laser system. The transmission data for all times and boxes for both models are plotted against the average box optical depth to obtain a profile of optical depth that a

laser could be transmitted through. Plots like these could be used as decision aids for laser system operators.

6.2 Conclusions

Cirrus clouds, no matter how thin, will affect laser transmission and those effects can somewhat be quantified with laser transmission models (Kolb et al. 2001). By examining a realistic RAMS-generated cirrus cloud data set and inputing average cloud properties into single and multiple layer laser transmission models, understanding of how cirrus affect laser transmission is gained.

- Ice crystal orientataion does have an effect on the laser power transmitted through a cirrus cloud. By examining sensitivity studies of the laser model it is clear that when all ice crystals are oriented in the horizontal the transmission is higher than when the orientation is random.

- Second order scattering contributions are negligible compared to the direct transmission. The cases where the second order scattering is run show that there is a contribution from scattering but that that contribution is very small.

- Transmission through cirrus clouds changes with the cloud as it develops. Examining the transmission through a particular band of cloud in a Lagrangian-like manner showed that as the band grew in optical depth the transmission through it decreased.

- Optical depth is not the only factor effecting laser transmission. Ice crystal size distribution and number concentration also will affect the amount of laser power transmitted through the cloud.

- The method used for averaging is very important. Errors can occur by including clear air in the averaging of optical properties of a cloudy space and such cases need to be handled with care.

Profiles of laser power transmission offer insight as to how much power will be received at a given target height whether it be below, within, or above the cloud layer.

By using average optical depth as a designator for each averaged cloud box, transmission is compared for a variety of optical depth conditions. With such information and cloud top and base values, laser system operators will have some idea of how a cloud of a given optical depth will affect laser transmission.

6.3 Future Work

This research has only scratched the surface of what is yet to be done. More cases of cirrus clouds need to be run through the current models to expand the parameter space of of optical depth vs. transmission. Other modeled cirrus cases such as cirrus uncinus, tropical cirrus, Arctic cirrus, cirrostratus, contrail cirrus, and additional mid-latitude cirrus should be examined with this laser transmission model and future versions of it. Such analysis can result in lookup tables as to what transmission profiles could be expected for a variety of cirrus conditions.

Tables of transmission including contributions of aerosol and water vapor should also be generated for realistic data on how a laser will be affected through the atmosphere. Clearly identifying ice crystal number concentrations and size distributions for each case will also be useful in determining how well a laser will be transmitted through a given cloud.

The laser transmission models are still in development. These models will be able to accept horizontal variations in the cloud field in the future. Better resolution cloud information in both the horizontal and vertical will be the culmination of the laser transmission model. The resolution of the cloud data will be the limiting factor for what can be achieved with the laser model. Perhaps data from GOES or other satellite instruments such as the AVHRR will be incorporated into the model to create real time transmission profiles which will serve as an atmospheric decision aid for laser system users.

High resolution cirrus forecasts could also be useful to an atmospheric descision aid and to laser ststem planners as as models are improved upon in the future. With such information, airborne laser systems can maximize their flight plans by avoiding areas most

likely to contain optically thick cirrus. Large eddy simulation (LES) models could also be useful in diagnosing turbulence within the cloud field to offer more insight to planners.

There is much still to be done to characterize the effects of cirrus on laser transmission. Many more cases of cirrus need to be examined for different regions and different times of the year. The transmission model needs to be upgraded to include horizontal variation and the data sources for the transmission model need to be identified. With laser systems becoming more and more prominent in the future, knowing the transmission through cirrus clouds will be imperitive to future operations.

Appendix A

LIST OF ACRONYMS

1-D	One Dimension
3-D	Three Dimensions
AVHRR	Advanced Very High Resolution Radiometer
CSU	Colorado State University
FIRE	First ISCCP Regional Experiment
GOES	Geostationary Operational Environmental Satellite
IRRS	Institute of Radiation and Remote Sensing
ISCCP	International Satellite Cloud Climatology Project
LES	Large Eddy Simulation
MAPS	Mesoscale Analysis and Prediction System
NOAA	National Oceanic and Atmospheric Administration
RAMS	Regional Atmospheric Modeling System
UCAR	University Corporation for Atmospheric Research
UCLA	University of California at Los Angeles
UTC	Universal Coordinated Time

Appendix B

EXTINCTION COEFFICIENT

B.1 Atmospheric particles

The atmosphere scatters light through interactions with molecules, aerosols, cloud droplets, and ice crystals contained within it. These particles are of various shapes and sizes and affect light differently. Molecules are by far the smallest particles with aerosols being larger and water drops and ice crystals being the largest. Each set of particles are governed by a different set of scattering theories; molecules by Rayleigh scattering, aerosols by Mie theory, and ice crystals and water drops by diffraction theory (Weichel 1989).

Molecules are the smallest particles found in the atmosphere and are much smaller than 0.1 μm. These particles scatter electromagnetic radiation according to Rayleigh scattering which is due to the displacement of bound electrons by the incident electric field. This type of scattering occurs when the size of the scattering particle is much smaller than the incident wavelength of light.

Aerosols are larger particles found in the atmosphere and come from both natural and anthropogenic sources. Table B.1 shows the different size classifications for aerosols. These particles scatter according to Mie theory. Mie scattering occurs when the particle size is on the order of the wavelength of incident light.

Cloud drops and ice crystals are the largest particles ranging from 1 μm for a small cloud droplet to 2 mm diameter of a large ice crystal. These particles are governed by diffraction theory since they are much larger than the wavelength of light. As the radius of a particle approaches 10λ, where λ is the wavelength, the extinction coefficient approaches the value of 2 and the scattering is independent of wavelength (Weichel 1989).

Table B.1: Table of aerosol by size according to Junge Classification.

| Aerosol Class	Size Range
Aitken Particles	r < 0.1 μm
Large Particles	0.1 < r < 1 μm
Giant Particles	r > 1 μm
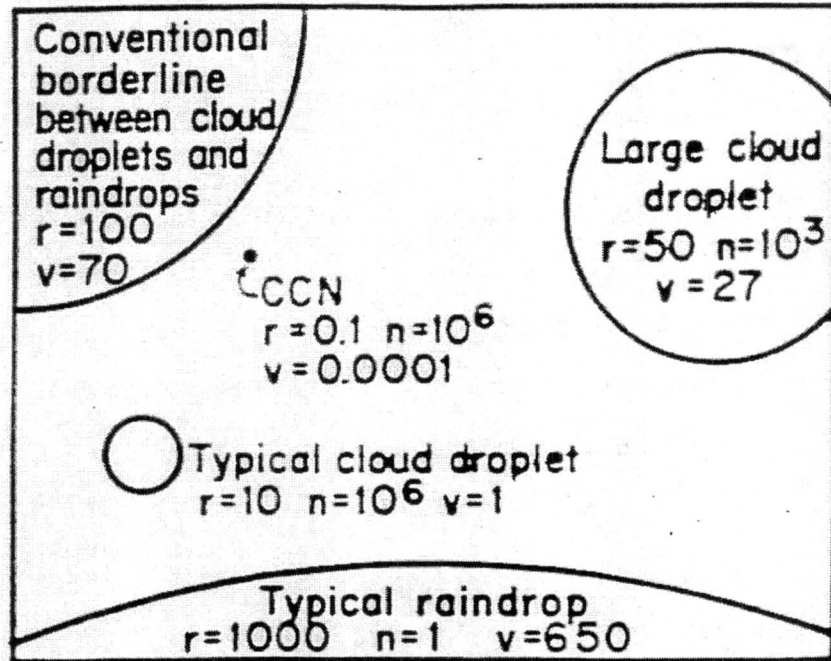
Figure B.1: Relative sizes of typical cloud and raindrops; r is the radius in micrometers, n is the number per liter of air, and v is the terminal fall speed in centimeters per second. (From McDonald, 1958)

B.2 Extinction

Assuming that these particles in the atmosphere scatter more than they absorb, extinction in the atmosphere, which is the sum of scattering and absorption, may be equated to the contributions of scattering (Bohren 1987).

An empirical equation that is used to determine the extinction coefficient of atmospheric particles is given in equation B.1.

$$Q_{ext} = C_1 \lambda^{-\delta} + C_2 \lambda^{-4} \qquad \text{(B.1)}$$

Where Q_{ext} is the extinction coefficient, C_1, C_2, and δ are constants determined by particle concentration and size distribution, and λ is the wavelength. For molecules, the λ^{-4} term, or the Rayleigh scattering term, is the dominant effect while aerosols have the $\lambda^{-\delta}$ term as the dominant one. For very large particles such as cloud drops and ice crystals, the value of δ approaches 0 (Weichel 1989).

The extinction coefficient is also related to the size parameter x.

$$x = \frac{2\pi r}{\lambda} \qquad \text{(B.2)}$$

Where r is the particle radius and λ is the wavelength. Figure B.2 shows a plot of extinction coefficient vs. size parameter and it gives an interesting result.
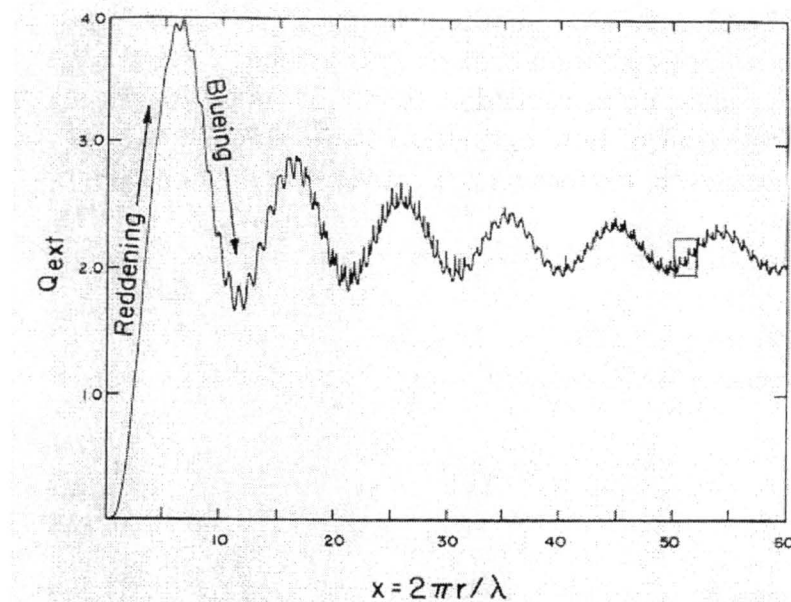

Figure B.2: Extinction efficiency for water drops in air calculated as a function of size parameter x (in μm) for wavelength $\lambda = 0.5$ μm. (From Stephens, 1994)

As seen in Figure B.2, the extinction coefficient rises to a maximum value of 4, then sinks to a minimum value, then damps out to the value of approximately 2 at large size parameters. This effect is known as the 'Extinction Paradox'. For large particles, the extinction coefficient is equal to the sum of the shadow area of the particle with the area filled by diffraction over the area of the particle (Stephens 1994). It is also possible to

create a plot by fixing the radius and varying the wavelength. This type of plot will be different from Figure B.2 due to changes in the refractive index. However at large size parameters the extinction coefficient is nearly independent of the wavelength.

Figure B.2 shows clearly how the size of a particle affects the amount of extinction. Rayleigh particles, such as atmospheric gases, are found near the 0 value of the size parameter where the extinction is very small. Aerosols fit in the size parameter regions from about 1 to 600 causing both reddening and blueing effects, which can be seen by Figure B.2, based on their size distributions. Cloud drops and ice crystals fit within the range of 100 to 30,000 which is well off the scale of this plot and the extinction coefficient is approximately 2. Since the value of extinction does not change much at such large size parameters, the extinction coefficient is independent of wavelength for cloud drops and ice crystals.

REFERENCES

Anderson, G. P., R. H. Picard, and J. H. Chetwynd, 1995: Proceeding of the 17th Annual Review Conference on Atmospheric Transmission Models, Special Report No. 274, Phillips Laboratory/Geophysics Directorate, Hanscom AFB, 332 pp.

d'Almeida, G. A., P. Koepke, and E. P. Shettle, 1991: *Atmospheric Aerosols, Global Climatology and Radiative Characteristics.* A. Deepack Publishing, Hampton, VA, 561 pp.

Benedetti, A. and G. L. Stephens, 2001: A new look at the evaluation of cirrus simulations using observations. *Atmos. Res.*, submitted.

Bohren, C. F., 1987: *Clouds in a Glass of Beer*, John Wiley & Sons, Inc., 195 pp.

Cheng, W. Y. Y., T. Wu, and W. R. Cotton, 2001: Large eddy simulations of the 26 November 1991 FIRE II cirrus case. *J. Atmos. Sci.*, **58**,1034–1034.

Clark, J. C., C. Mitrescu, and W. R. Cotton, 1999: LES derived vertical velocity spectra of fog and cirrus. *13th Symposioum on Boundary Layers and Turbulence, AMS*, Dallas, TX.

Cotton, W. R. and R. A. Anthes, 1989: *Storm and Cloud Dynamics*, Academic Press, 883 pp.

Eaton, F. D., G Nastrom, B. Masson, I. Hahn, K. McCrae, S. Nowlin, and T. Berkopec, 1998: Radar and aircarft observations of a layer of strong refractiviy turbulence, *Paper no. 3381-32, SPIE Aerosense Conference, Airborne Laser Advanced Technology*, Orlando, FL.

Fu, Q., and K. N. Liou, 1992: On the correlated k-distribution method for radiative transfer in non homogeneous atmospheres. *J. Atmos. Sci.*, **49**, 2139–2156.

Hahn, I. L., B. P. Venet, F. D. Eaton, R. J. Hugo, and S. R. Nowlin, 1999: Refractive index structure parameter in the boundary layer as measured from an aircraft and ground based scintillometer. *13th Symposioum on Boundary Layers and Turbulence, AMS*, Dallas, TX.

Hansen, J. E., and L. D. Travis, 1974: Light scattering in plantary atmospheres. *Space Sci. Rev.*, **16**, 527–610.

Harrington, J. Y., M. P. Meyers, R. L. Walko, and W. R. Cotton, 1995: Parameterization of ice crystal conversion processes due to water vapor deposition for mesoscale models using double-moment basis functions. Part I: Basic formulation and parcel model results. *J. Atmos. Sci.*, **52**, 4344–4366.

Harrington, J. Y., T. Reisin, W. R. Cotton, and S. M. Kreidenweis, 1999: Cloud resolving simulations of arctic stratus. Part II: Transition-season clouds. *Atmos. Res.* **51**, 45–75.

Heymsfield, A. J., and R. G. Knollenberg, 1972: Properties of cirrus generating cells. *J. Atmos. Sci.*, **29**, 1358–1366.

Hobbs, P. V., L. F. Radke, and D. G. Atkinson, 1975: *Airborne Measurements and Observation in Cirrus Clouds.* AFCRL-TR-75-0249, Air Force Geophysics Laboratory, Hanscom AFB, 117 pp.

Jayaweera, K. and B. J. Mason, 1965: The behavior of freely falling cylinders and cones in a viscous fluid. *J. Fluid Mech.*, **22**, 709–720.

Kolb, I. L., W. Y. Y. Cheng, and W. R. Cotton, 2001: Laser transmission through simulated cirrus clouds by one-layer and multiple layer propagation models. *AIAA-2001-2795, 32nd Plasmadynamics and Lasers Conference, AIAA*, Anaheim, CA.

Liou, K. N., 1972: Light scattering by ice clouds in the visible and infrared: A theoretical study. *J. Atmos. Sci.*, **29**, 524–536.

Liou, K. N., 1986: Influence of cirrus clouds on weather and climate processes: A global perspective. *Mon. Wea. Rev.*, **114**, 1167–1199.

Liou, K. N., Y. Takano, S. C. Ou, A. Heymsfield, and W. Kriess, 1990: Infrared transmission through cirrus clouds: A radiative model for target detection. *ZAppl. Opt.*, textbf29, 1886–1896.

Liou, K. N., 1992: *Radiation and Cloud Processes in the Atmosphere*, Oxford University Press, 497 pp.

Liou, K. N., Y. Takano, S. C. Ou, 1999: Laser transmission through cirrus clouds, Interim report 1 Oct 98 - 30 Sep 99. Airborne Laser System Program Office, Kirtland AFB, 66 pp.

Liou, K. N., Y. Takano, S. C. Ou, M. W. Johnson, 2000: Laser transmission through thin cirrus. *Appl. Opt.*, **39**, 4886–4894.

Lutgens, F. K. and E. J. Tarbuck, 1992: *The Atmosphere, An Introduction to Meteorology*, Prentice Hall, 430 pp.

McDonald, J. E., 1958: The physics of cloud modification, *Advances in Geophysics*, /textbf5, pp.223-303, Academic Press, New York.

Mace, G. G., D. O'C. Starr, T. P. Ackerman, and P. Minnis, 1995: Examination of coupling between an upper-tropospheric cloud system and synoptic-scale dynamics diagnosed from wind profiler and radiosonde data. *J. Atmos. Sci*, **52**, 4094–4127.

Masson, B., B. Scruggs, M. Hayes, J. Wissler, K. Bishop, and D. Kyrazis, 1996: Airborne measurement of tropopausal temperature fluctuations. *AIAA-96-0265, 34th Aerospace Sciences Meeting and Exhibit, AIAA*, Reno, NV.

Meyers, M. P., R. L. Walko, J. Y. Harrington, and W. R. Cotton, 1997: New RAMS cloud microphysics parameterization. Part II: The two-moment scheme. *Atmos. Res.*, **45**, 3–39.

Minnis, P., K. N. Liou, and Y. Takano, 1993: Inference of cirrus cloud properties using satellite-observed visible and infrared radiances. Part I: Parameterization of Radiance Fields. *J. Atmos. Sci.*, **50**, 1279–1304.

Ono, A., 1969: The shape and riming properties of ice crystals in natural clouds. *J. Atmos. Sci.*, **26**, 138-147.

Ou, S. C., K. N. Liou, Y. Takano, N. X. Rao, Q. Fu, A. J. Heymsfeld, L. M. Miloshevich, B. Baum, and S. A. Kinne, 1995: Remote sounding of cloud optical depths and ice crystal sizes from AVHRR data: Verification using FIRE II IFO measurements. *J. Atmos. Sci.*, **52**, 4143–4158.

Pielke, R. A., W. R. Cotton, R. L. Walko, C. J. Tremback, W. A. Lyons, L. D. Grasso, M. E. Nicholls, M. D. Moran, D. A. Wesley, T. J. Lee, and J. H. Copeland, 1992: A comprehensive meteorological modeling system - RAMS. *Meteorol. Atmos. Phys.*, **49**, 69–91.

Platt, C. M. R., N. L. Abshire, and G. T. McNice, 1978: Some microphysical properties of an ice cloud from lidar observation of horizontally oriented crystals. *J. Appl. Meteor.*, **17**, 1220–1224.

Rothman, L. S., R. R. Gramache, R. H. Tipping, C. P. Rinsland, M. A. H. Smith, D. C. Benner, V. M. Devi, J.-M. Flaud, C. Camy-Peyret, A. Perrin, A. Goldman, S. T. Massies, L. R. Brown, and R. A. Toth, 1992: The HITRAN molecular database: Editions of 1991 and 1992. *J. Quant. Spectrosc. Radiat. Transfer*, textbf48, 469–507.

Stephens, G. L., 1994: *Remote Sensing of the Lower Atmosphere*, Oxford University Press, 523 pp.

Stone, R. S., G. L. Stephens, C. M. R. Platt, and S. Banks, 1990: The remote sensing of thin cirrus cloud using satellites, lidar and radiative transfer theory. *J. Appl. Meteo.*, **29,** 353–366.

Takano, Y. and K. N. Liou, 1989a: Solar radiative transfer in cirrus clouds. Part I: Single-scattering and optical properties of hexagonal ice crystals. *J. Atmos. Sci.*, **46,** 3–19.

Takano, Y. and K. N. Liou, 1989b: Solar radiative transfer in cirrus clouds. Part II: Theory and Computation of Multiple Scattering in an Anisotropic Medium. *J. Atmos. Sci.*, **46,** 20–36.

Takano, Y. and K. N. Liou, 1995: Radiative transfer in cirrus clouds. Part III: Light scattering by irregular ice crystals. *J. Atmos. Sci.*, **52,** 818–837.

Varley, D. J., I. D. Cohen, and A. A. Barnes, 1980: *Cirrus Particle Distribution Study, Part VII.* AFGL-TR-80-0324, Air Force Geophysics Laboratory, Hanscom AFB, 82 pp.

Weichel, H., 1989: *Laser Beam Propagation in the Atmosphere*, SPIE Optical Engineering Press, 98 pp.

Weickmann, H. K., 1945: Formen and bildung atmosphärisher eiskristalle. *J. Meteor.*, **28,** 12–52.

Wu, T., 1999: Numerical Modeling Study of the November 26, 1991 Cirrus Event. Ph.D. dissertation, Colortado State University, Fort Collins, CO, 186 pp.

Wu, T., W. R. Cotton, and W. Y. Y. Cheng, 2000: Radiative effects on the diffusional growth of ice particles in cirrus clouds. *J. Atmos. Sci.*, **57,** 2892–2904.